CALT-68-630
DOE RESEARCH AND
DEVELOPMENT REPORT

Recent Experimental Results on High Transverse Momentum Scattering from Fermilab*

G. C. FOX

California Institute of Technology, Pasadena, California 91125

ABSTRACT

A survey of recent high transverse momentum ($p_\perp$) scattering experiments at Fermilab concentrates on a comparison of three experiments that use a "jet" (i.e., sum over several particles) $p_\perp$ trigger. We also discuss two particle correlations and ϕ production.

Invited talk presented at Argonne APS meeting,
Argonne, Illinois, October 1977.

*Work supported in part by the U.S. Department of Energy under Contract No. EY76-C-03-0068.

I. Introduction

Until recently, the only results from Fermilab on high $p_\perp$ scattering came from single particle inclusive experiments. In particular, we have the charged particle measurements of the Chicago-Princeton group[1] and the π^o cross sections from the Berkeley-Brookhaven-Caltech collaboration[2]. The former has a proton beam and both hydrogen and nuclear targets; the latter has π and proton beams on a hydrogen target. These important data, combined, of course, with the extensive results from the ISR[3,4], have been used to study $p_\perp$, energy s and particle species dependence of high $p_\perp$ processes. The resulting picture was summarized by Frisch last year[5] and so I will not discuss these single particle measurements here.

There are five experiments from Fermilab that have reported data in the past year. The first, discussed in Section III, measures ϕ production up to $p_\perp$ of 3 GeV/c in 400 GeV/c pBe collisions[6]. As we will see, these data are consistent with simple estimates based on the measured ρ, K and π yields at the same $p_\perp$. The next experiment, to be discussed in Section IV, measures two particle "back to back" correlations with good statistics up to $p_\perp$ of 5 GeV/c[7,8]. These data address the atomic number, particle-species and $p_\perp$ dependence of the two particle cross-section. Finally, in Section V, we compare the results of three jet trigger experiments[9-12]. These experiments, which study groups of particles that sum up to high $p_\perp$, now see most of the properties expected if jets are identified with the fragmentation of constituents (quarks)[13-17]. Before the three experimental sections, we briefly discuss a theoretical framework in Section II.

II. Necessary Theory

In order to discuss the data, it is convenient to have some theoretical motivation and I shall use the quark scattering model[13-17]. Although the

present formulation is surely not the final word, this model does provide a qualitatively reasonable description of both the single particle and correlation data at high $p_\perp$.

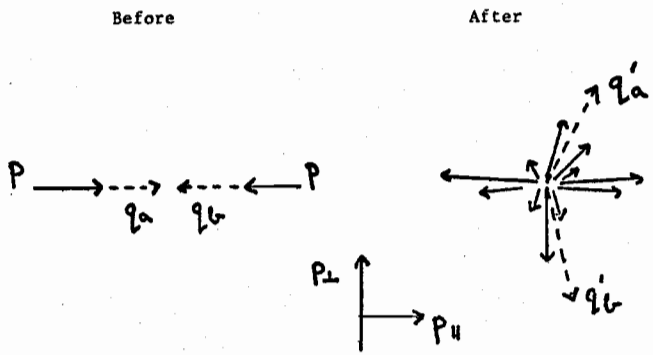

This model leads to events with a four jet structure. Jets or groups of particles come from the fragmentation of q'_a (the scattered quark q_a) and q'_b (the scattered quark q_b). There are two further jets from the fragmentation of the remaining stuff in the beam and target.

A typical hadron h fragmenting from quark q'_a or q'_b has momentum $z\ p_\perp^{quark}$ along the quark direction and $\underline{k}_\perp$ perpendicular to it ($0 \le z \le 1$).

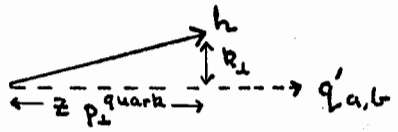

Explicit calculation shows that a single particle trigger for $p_\perp > 2$ GeV/c takes on the average 80 to 90% of the quark's q'_a momentum (i.e., z for trigger hadron is 0.8 to 0.9). In this model, a single particle trigger is just a very biased and unusual fragmentation of the quark q'_a. In the unbiased fragmentation, the average particle has a $z \approx 0.2$. In the quark scattering model, a jet is a collection of such typical particles of rather low momentum ($\langle z \rangle = 0.2$ implies for $p_\perp^{quark} = 5$ GeV/c, a mean transverse momentum of the hadrons in a jet of 1 GeV/c) whose sum is the transverse momentum of the quark q'_a.

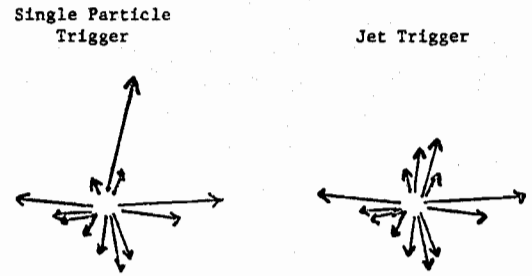

For either jet or single particle trigger, one sees on the away side, the unbiased fragmentation of the quark q'_b. The transverse momentum of an away side hadron is given by,

$$p_\perp^{\text{away hadron}} \sim z\ p_\perp^{q'_b} = z\ p_\perp^{q'_a} \sim \frac{z}{z_{\text{trigger}}}\ p_\perp^{\text{trigger hadron}} \quad : \text{Single Particle Trigger}$$

$$= z\ p_\perp^{\text{jet}} \quad : \text{Jet Trigger}$$

As the mean value of $z_{trigger}$ is roughly independent of $p_\perp^{trigger\ hadron}$, one expects the distributions of

$$z_J = \frac{p_\perp^{away\ hadron}}{p_\perp^{jet}} = z \qquad \text{: Jet Triggers}$$

and z_p (also called x_e) $= \dfrac{p_\perp^{away\ hadron}}{p_\perp^{trigger\ hadron}} \propto z$, : Single Particle Triggers

should scale, i.e., be independent of trigger $p_\perp$, if as expected the quark's fragmentation depends only on z and not on its momentum. z_p is properly defined only using components in the plane defined by the beam, target and trigger hadron. However, in the application in Section IV, the acceptance of the apparatus essentially forces coplanarity of the particles and this nicety is unimportant.

As is now well known[16,18,19], the effects of the parton transverse momentum inside the initial hadrons is quantitatively very important. In particular, the configuration where the partons' transverse momenta point towards the trigger (whether jet or single particle) is always enhanced.

Enhanced Configuration

This has the effect that the mean transverse momentum of q_b' is less than that of q_a'. However, although the magnitude of the z_J and z_p distributions are affected, the prediction of scaling with trigger $p_\perp$ is still approximately valid.

I will also refer to the momentum p_{out} of the away side hadron perpendicular to the plane defined by beam, target and trigger. In a hard scattering model, the p_{out} distribution should be limited; the detailed predictions for this distribution are given in Refs. 16), 18) and 19).

I will occasionally refer to the detailed calculations of Ref. 16) (called FFF). They give only qualitative agreement with data but they provide a useful way to compare experiments taken under different kinematic conditions. A better understanding of the data which combines the ideas of Refs. 16), 17) and 19) should soon be available[20] but it is not necessary for this paper.

III. ϕ Production at High $p_\perp$

These data[6] come as a byproduct of a two arm spectrometer search for charmed particle production in $K^{\mp}\pi^{\pm}$ and other two charged particle decay modes.

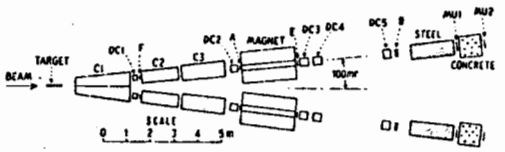

The apparatus, which was situated in the M2 beam line at Fermilab, is shown above where C1, C2, C3 are Cherenkov counters and DC1-5 drift chambers. A-F, MU1 and MU2 are scintillation counters. At the incident energy of 400 GeV/c, the 100 milliradian setting of each arm corresponds to an angle slightly backward of 90° in the center of mass. The ϕ is observed through the K^+K^- decay mode where <u>both</u> kaons traverse the <u>same</u> arm of the spectrometer.

The resultant ϕ cross-section is plotted in Fig. 1 as a ratio of ϕ to π^- production. This level of ϕ production contributes about 2% of the observed prompt μ production[6]. Also on Fig. 1, we show the predictions for this quantity

from the quark fragmentation model of Field and Feynman[17]. The agreement is impressive above $p_\perp$ of 2 GeV/c. The success of the model can be understood qualitatively. Thus, the ISR has shown that the ratio of ρ to π production is about unity[22]. The ϕ meson needs two strange quarks and so we can estimate this from K production which only needs one.

$$\phi/\pi = (\rho/\pi)\cdot(\phi/\rho) \approx (\rho/\pi)\cdot(K/\pi)^2$$

which for $(K^-/\pi^-) \sim 0.25$ (the value in this $p_\perp$ range[1]) gives roughly the observed rate. In fact, replacing ϕ by ψ and K by the charmed D meson, the above equation has often appeared in experimental proposals as an estimate of D meson production (an estimate which seems larger than current upper limits[21]). The Field-Feynman curve in Fig. 1 comes from a beautiful model for quark fragmentation which includes our naive argument above in a quantitative fashion. This ϕ production cross-section is only one of a multitude of tests that are possible of this model in lepton and hadron processes.

The data in Fig. 1 are substantially lower than the theory below $p_\perp$ of 2 GeV/c. This could be due to the presence of a different dynamical mechanism that produces pions far more profusely compared to ϕ's than quark fragmentation does. This is not unreasonable as $p_\perp$ = 2 to 3 GeV/c is normally considered the start of the high transverse momentum regime. Another possibility is that the $p_\perp$ < 2 GeV/c particles come from the fragmentation of such low momentum quarks that the Field-Feynman model is inapplicable (perhaps because of mass effects that are ignored in their current model). It would be interesting to look at ϕ production in e^+e^- collisions as a function of center of mass energy.

Observing the ϕ in one arm of the two arm spectrometer, the experimentalists can look at particles in the second arm. Interestingly enough, they see no significant enhancement of the K/π ratio in the second arm for the ϕ triggers

compared to pions in the first arm. This agrees with the quark scattering approach, where there <u>are</u> expected to be more K's in events containing a ϕ but these K's are on the same side as the trigger and not on the away side probed by the second arm. We will return to such quantum number correlations in the next section where they are studied at higher $p_\perp$.

IV. Two Particle Correlations

The data from Fermilab experiment 494 in the proton area, also come from a two arm spectrometer which is sketched below[7,8].

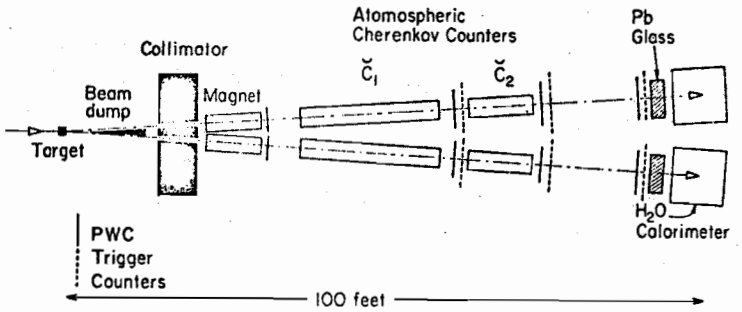

Charged particles, emitted back to back, at approximately 90° in the center of mass, are momentum analyzed and (partially) identified by two Cherenkov counters in each arm. The apparatus has a very small azimuthal (±3°) acceptance but a reasonable longitudinal bite (θ = 72° to 108° in c.m. at 400 GeV). An energy threshold in a water hadron calorimeter served to beat down the low $p_\perp$ background in a $p_\perp$ trigger that was otherwise specified by the value of the magnet setting. Not only is the apparatus similar to that in the previous

section but these high $p_\perp$ data were also obtained as a byproduct of more "exciting" physics (in this case, lepton pair production[23]). The values of $p_\perp$ reached in E494 were substantially higher than those in the ϕ experiment.

The data were taken with a Beryllium and Tungsten target. Previous studies of single particle inclusive measurements[1] had shown that the Atomic number A dependence could be parameterized as

$$Ed^3\sigma/d^3p \propto A^\alpha$$

where the parameter α depends on both the $p_\perp$ and species (π, K or p) of the produced particle. α rises above the naive value of 1 for incoherent scattering off nucleons in the target, for $p_\perp > 2$ GeV/c. The new E494 results are shown in Fig. 2 where a similar behavior is seen for the two particle data as long as it is plotted against the transverse momentum $p_{\perp N}$ of the <u>dihadron</u> pair.

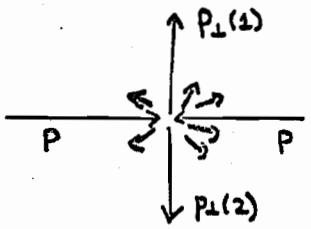

i.e., $p_{\perp N} = |p_\perp(1) - p_\perp(2)|$

In the quark scattering picture, I can see no reason why $p_{\perp N}$ in the two particle case should be analogous to $p_\perp(1)$ in the single particle cross-section. These data are plotted in a different way in Fig. 3 where $1/N\ dN/dz_p$ is plotted for a fixed value of $p_\perp(1)$. Here z_p is just $p_\perp(2)/p_\perp(1)$. For $z_p > 0.5$, this distribution is lower for the tungsten compared to the Beryllium target. For these z_p, we have a smaller $p_{\perp N} = |1-z_p|\ p_\perp(1)$ than $p_\perp(1)$ and the α governing

the dN/dz_p's atomic number dependence is lower than the α for the single particle cross section (i.e., N in $1/N\ dN/dz_p$). Correspondingly in Fig. 3, we see that $1/N\ dN/dz_p$ is lower for the tungsten compared to the Beryllium target data. Expressed this way, one can see that one possible explanation of the pair v. single particle α dependence is that the mean quark transverse momentum is larger in the heavy compared with the light nucleus. This hypothesis simultaneously gets $\alpha > 1$ for the single particle cross-section and a lower $1/N\ dN/dz_p$ with increasing atomic number. On the other hand, I don't see how this "explanation" predicts the species dependence of α seen in Ref. 1. A (quark) multiple scattering model, which does give $\alpha > 1$ in the single particle triggers, does not seem to predict the atomic number dependence of $1/N\ dN/dz_p$. (The away and trigger sides are symmetric in this model. Both can multiple scatter.)

In Figs. 4 and 5, we study the z_p distributions. As shown in Fig. 5, the FFF theory has about the right shape but is about a factor of three high in overall normalization. Thus in Fig. 4, we have arbitrarily divided the theory by a z_p independent factor. The data have the same $p_\perp$ and z_p dependence for trigger $p_\perp$ greater than about 3.5 GeV/c. The rise in the theory (and experiment) with $p_\perp$, seen in Fig. 4, is due to the acceptance of the spectrometer; the theory would rise by about 10% from trigger $p_\perp$ of 2.5 to 6 GeV/c if the unbiased away side distribution was plotted. Dividing the data by the theory, we get an (model dependent) acceptance corrected z_p distribution; it falls with $p_\perp$ up to $\sim$ 3.5 GeV/c and then scales (i.e., is approximately independent of $p_\perp$) for larger $p_\perp$. This picture is in nice agreement with the ISR data from the CCHK and British-French-Scandinavian (BFS) groups[4,19,24] shown in Figs. 6 and 7. The nonscaling term for $p_\perp \leq 3.5$ GeV/c could well be due to the contribution of the spectators (i.e., fragments of beam and target jets) as in

the CCHK model[19]. Actually, not only is the trigger $p_\perp$ dependence of the z_p distributions similar in the new Fermilab and ISR data, but the discrepancy between the FFF predictions and the data is about the same (a factor of 3). This is now true for CCHK[19], BFS[4,24], CCRS[25] (see Ref. 18 for a comparison of FFF with CCRS), and E494[8], although the discrepancy between theory and experiment is not a universal factor. For instance, both BFS and E494 indicate that the experimental z_p dependence is slightly sharper than that predicted by FFF. This seems to disagree with Figs. 6(a,b) where the FFF predictions actually get closer to the CCHK data as z_p goes from 0.5 to 1. In any case, it is clear that the FFF theory needs substantial modification[20]. However, the important feature of all these data is that scaling does appear to set in at large $p_\perp$; approximate scaling is predicted in all hard scattering models and it would appear that the region $p_\perp \geq 3.5$ GeV/c is appropriate for application of such models.

In Fig. 8, we study the dependence of the away side, integrated for $z_p \geq 0.75$, on the species of both the trigger and away side particle. Most of the thirty-six possibilities (coming from the six trigger and six away side species) are shown in the figure. One's first impression is that the away side species dependence is, in absolute cross-section, independent of trigger species. Further, the ratios of different away side species are the same as the single particle cross-section ratios (indicated by the wavy lines at the side of the figure). This simple picture is just that predicted by the quark scattering model but a closer look reveals some deviations from it. First K^-, p and $\bar{p}$ triggers, seem to have a lower rate on the away side for all away side species. Two exceptions to this are K^- trigger, K^+ away and proton trigger, anti-proton away configurations which are at about the same level as the other trigger species. Considering ratios to π's observed on the away side, we see that $K^-K^+/K^-\pi$ and $p\bar{p}/p\pi$ are enhanced compared to $\pi K^+/\pi\pi$ and $\pi\bar{p}/\pi\pi$ by about a factor

of two (here we write trigger species followed by that on the away side). This structure is just what one might expect from the constituent interchange model (CIM)[26], but I don't know if the observed effect is of the expected size. Returning to Fig. 8, we see that not only do K^-, p and $\bar{p}$ seem to have less particles on the away side when they trigger, but also that when $\pi^\pm$ or K^+ trigger, there are fewer K^-, p, $\bar{p}$ on the away side than expected from ratios of single particle yields. This would happen if K^-, p and $\bar{p}$ triggers had two components, where the first is similar to $\pi^\pm$ and K^+ and gives the same away side distributions. If a second component gave essentially no large z particles on the away side, one would simultaneously explain both the overall away side reduction when K^-, p or $\bar{p}$ trigger and the reduced K^-, p, $\bar{p}$ away side yield for $\pi^\pm$ and K^+ triggers. (Note that as $z_p \sim 1$ in Fig. 8, this symmetry is almost trivial and it is important to see if it preserved when the z_p cut is reduced below 0.75.) It would be surprising if these two components had the same $x_\perp$ and $p_\perp$ dependence and it would be interesting to extend the E494 measurements to different kinematic regions. One can compare E494 with the results from the BFS experiment shown in Fig. 9. This ISR experiment can only study the charge dependence on the away side. They see a similar K^- trigger positive charge on away side correlation to the K^-K^+ effect in E494. There are differences in detail as E494, unlike BFS, sees no increase in positives on away side for K^- compared to π^- triggers; rather, they see a decrease in negatives on away side. Both E494 and BFS see interesting anomalies for $\bar{p}$ triggers; however, they are again different in detail. Clearly, further experimental study is needed.

V. Jet Experiments

The jet experiments were originally proposed four years ago - stimulated by the early data from the ISR and the first runs of the Chicago-Princeton group[1] at Fermilab. Both the structure of the events on the away side at the

ISR and the theoretical work of BBK[13] and Ellis and Kislinger[14] suggested that it would be useful to measure the yield at high $p_\perp$ of the production of groups (or jets) of particles whose momenta sum up to give the observed $p_\perp$. The jets are identified by a segmented calorimeter which measures the energies E_i of particles entering in it; the segmentation gives their angle θ_i and typically a trigger $p_\perp$ is formed as

$$p_\perp^{raw} = \sum_i E_i \theta_i$$

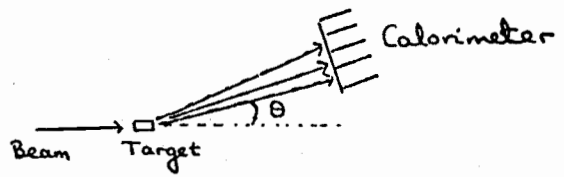

At 200 GeV/c, $\theta_i \sim 100$ milliradians (for 90° cms triggers) and one sees around 5 particles in calorimeter with a total energy of 50 GeV/c (for $p_\perp = 5$ GeV/c in E260). The calorimeters consist of a lead scintillator sandwich (to measure the electromagnetic part of showers) followed by an iron scintillator sandwich to detect the hadronic showers. This construction enables one to distinguish π^o's (with their electromagnetic showers) from the other hadrons.

The three jet experiments, which I will call by their Fermilab experiment numbers E236, 260 and 395 are compared in Table I and Figs. 10 and 11. The different experiments have calorimeters of different acceptance (Fig. 11) and, hence, may be sensitive to jets of different size. Further, they each have additional and different hardware to understand the jet and nonjet particles (Fig. 10). The results of the three experiments address both the size of the jet cross-section and the structure of the jet events. In each experiment, a jet vector

Table I: Comparison of Fermilab Jet Experiments

	E236	E260	E395
Coverage of Calorimeter in cms	2-1/2 str. (at 200 GeV/c)	1 str. (at 200 GeV/c) (two such)	2 str. and 1-1/2 str. (at 400 GeV/c)
Calorimeter Hadron Resolution at 20 GeV/c (all 3 expts. good at π^o's).	15% σ	23% σ but improves to 1.5% using spectrometer for charged particles but not for n,K_L^o.	20% σ
Calorimeter Segmentation. See Fig. 11.	6x, 10y strips. No x,y correlation.	4 x strips. y measured by light attenuation (equivalent to 5 y bins). x,y correlation if 1 particle into strip (but mean multiplicity in calorimeter ~ 5).	"Fly's eye" construction - each module gives x,y.
Beam Energies GeV. ( ) = no data available now.	(100 → ~400)	(130), 200	200, 400
Additional bells and whistles. See Fig. 10.	Single particle spectrometer on away side with $\check{C}$ identification.	Charged Particle Spectrometer with roughly full acceptance for $x_{\parallel} \geq 0$. Cherenkov information but not analyzed yet.	Two Segmented Calorimeters. Sensitive to 2 jet events.
Refs.	9	10, 11	12
Participating Institutions	Washington Fermilab Tufts	Caltech UCLA Fermilab UICC Indiana	Fermilab Lehigh Penn Wisconsin

is defined by the (three) vector sum of all particles entering the calorimeter and the jet $p_\perp$ is the transverse component of this jet vector. The three experiments agree that the jet cross section is large but as there are important differences in detail and the discussion is sensitive to the calorimeter acceptance, I will postpone this until last. First, I will discuss the structure of jet events where so far the only results available come from E260 (who use their large aperture multiparticle spectrometer to study charged particles in jet events) and E395. The latter use their segmented calorimeters to identify particles within the trigger and away side jet. The experiments are complementary; E260 does a very good job on charged particles and relatively poorly on neutrals while E395 does reasonably well on both charged and neutral particles. Essentially, all features expected of jets that correspond to fragmentation of constituents have been seen, i.e., the data agree with the qualitative predictions of models like that described in II where the constituents were taken to be quarks. However, some of the results are still not statistically very significant. Further, we need more studies both to take out trigger bias of the calorimeters and to distinguish jets from "random" collections of multiparticle systems. Some expected properties of jets produced by constituent scattering are:

A: Events are coplanar
B: There are 2 (trigger and away) jets per event (plus beam and target fragments, of course).
C: Transverse momentum of particles in a jet wrt its axis is limited.

} expected in all hard scattering models

D: Momentum distributions of particles within a jet are similar to those in e^+e^- and νp scattering (evidence that constituents are quarks?).

E: Away side distributions are similar for single particle and jet triggers (single particles and jets governed by similar dynamical mechanism).

F: Constituents have large internal transverse momentum. This is as seen in dimuon data[27] and needed to fit single particle high $p_\perp$ data (e.g., the low values of $1/N\ dN/dz_p$ for $z_p \gtrsim 0.5$ in Section IV and Refs. 16, 18, 19).

I will now discuss these jet properties and then finally in Section G, go onto the jet cross-section.

A. Coplanarity of Events (E260, Refs. 10, 11)

The underlying $2 \to 2$ scatter in constituent models suggests that all the particles in an event should define a plane such that the components of momenta out of this plane are only a few hundred MeV/c. This was tested by E260 using the sphericity analysis introduced by the SPEAR group[28].

As illustrated in Fig. 12(a), the axes x' and y' are found on an event by event basis in such a way as to minimize the root mean square component in the y' direction. Formally, x' and y' are the eigendirections of the matrix formed from the x and y components of momenta

$$T = \begin{bmatrix} \Sigma p_x^2 & \Sigma p_x p_y \\ \Sigma p_x p_y & \Sigma p_y^2 \end{bmatrix}$$

where the sum Σ runs over all charged particles in the event. The eigenvalues of T are called λ^2_{min} (or $\lambda^2_{y'}$) and λ^2_{max} ($\lambda^2_{x'}$).

In Fig. 12(b), the mean value of $|p_{y'}|$ is plotted against $|p_{x'}|$ for the trigger side ($p_{x'} > 0$) and away side ($p_{x'} < 0$). E260 has both a jet trigger and a single particle trigger based on one of the four x modules in calorimeter (Fig. 11) only. The latter trigger is often fooled by more than one particle but the single particle data presented only use events where the spectrometer reconstructed a high $p_\perp$ particle. For both single

particles and jets, we see in Fig. 12(b) strong and similar collimation in terms of the low value of $\langle p_{y'} \rangle / |p_{x'}|$; for instance, with $|p_{x'}| \sim 3$ GeV/c, $\langle p_{y'} \rangle$ is $\lesssim 0.35$ GeV/c. In Fig. 13, the distributions in $|p_{x'}|$ and $|p_{y'}|$ are shown separately for away and trigger sides in jet events. The sharp cutoff in $p_{y'}$ (mean $|p_{y'}| \sim 200$ MeV/c) is evident and is in contrast with slow fall in $p_{x'}$ on both trigger and away side. Finally in Fig. 14, we show the mean values of the eigenvalues of T. $2\lambda_{min}/(\lambda_{max}+\lambda_{min})$ is the analogue of sphericity introduced in Ref. 28. Low $p_\perp$, i.e., "normal" events, shown in Fig. 14(a) show a "sphericity" ~ 0.7 with λ_{max} about 0.4 bigger than λ_{min}; this agrees quite well with a simple Monte Carlo calculation assuming uncorrelated production. The jet events in Fig. 14(b) show about the <u>same</u> λ_{min} values as the low $p_\perp$ events but a λ_{max} that is substantially larger. This shows clearly that the jet events achieve high $p_\perp$ by large momenta in a plane (defined by x' and beam) without significant increase in components of momenta out of it. This observation agrees nicely with constituent models and is in disagreement with a fireball picture.

Although the sphericity method is optimal for demonstrating coplanarity, it does introduce a bias for λ_{min} is forced to be less than λ_{max}. The magnitude of this bias was investigated (Fig. 14(a)) but still one is left with an uneasy feeling. Future analysis should also study $p_{y'}$ with respect to a less optimal but less biased set of axes. (Defining x' as the single particle or jet direction is perhaps best.)

B. <u>Trigger and Away Side Jets</u> (E395, Ref. 12)

As indicated in Table I, E395 has one good size (the "right") and one medium (the "left") calorimeter. Jet triggers were taken with both

of them. A good study of the away side is possible by triggering on the poorer "left" calorimeter and studying, in an unbiased way, the distribution in the "right" calorimeter. Their results are illustrated in Fig. 15 where the away side $p_\perp$ distribution is plotted for two trigger $p_\perp$ values. In each case, there is a clear, but broad, peak in the away side distribution whose position shifts up with increasing trigger $p_\perp$. In Fig. 15(c), we see that the away side $p_\perp$ increases nicely with trigger $p_\perp$ although it always lies below it in value. The interpretation of these data is hard without detailed Monte Carlo calculations. Presumably, transverse momentum is conserved, and if the away side calorimeter covered all (2π str.) and not just 2 str. of the away side, it would see full balancing. One must show that the away side jets have the same internal clustering properties and momentum make-up (Sections C, D) as trigger jets. E395 do observe that 25% (low trigger $p_\perp$) to 40% (high trigger $p_\perp$) of "left" triggers have away side jet vectors that lie in middle 0.1 str. (20° in θ_{cms} x 20° in ϕ) of the "right" calorimeter. This supports the jet interpretation for the away side signal, but, of course, any random collection of particles in a finite, symmetrically placed, detector will tend to have a total vector that points towards the middle of detector. Ignoring these doubts, the naive interpretation of Fig. 15(c) is that $p_\perp^{\text{away jet}} < p_\perp^{\text{trigger jet}}$ which is the result anticipated in Section II from the internal momentum of constituents inside the hadron.

E260 also has two calorimeters but their poorer acceptance reduces the efficiency for detection of both jets; however, it should also be possible to study two jet events in the E260 data as well.

C. Internal Clustering of Jet Members (E260, Ref. 10; E395, Ref. 12)

In constituent models, the component of momentum $k_\perp$ perpendicular to the jet vector should be small and similar to value ($k_\perp \sim 330$ MeV/c) seen in SPEAR jets[28]. In E260, one sees[10] a mean $\langle k_\perp^2 \rangle = 0.12$ (GeV/c)^2 smaller than the expected 0.17 value. This reduction could be partly due to the fact that we are measuring $k_\perp$ wrt a jet vector defined using the same group of particles for which we are finding the $k_\perp$. (As E260 sees ~ 5 particles in a jet, this bias would reduce $\langle k_\perp^2 \rangle$ by $\sim 20\%$ from its true value.) Another problem in E260 is that the small calorimeter acceptance leads to a loss of high $k_\perp$ (especially at low z) particles. The latter problem is not present in E395 and we show some preliminary data in Fig. 16. The distributions in cms angle α, between particle and jet vector, ($\tan\alpha = k_\perp/zp_\perp^{jet}$) show a clear sharpening as $p_\perp^{jet}$ increases. This is, of course, what you would expect if $\langle k_\perp \rangle$ is fixed as $p_\perp^{jet}$ increases. The value of $\langle k_\perp \rangle$, in Fig. 16, looks a little larger, $\gtrsim 400$ MeV/c, than expected. However, E395 could well have the opposite bias to E260; namely, the larger acceptance calorimeter could include low momentum particles from beam and target jets that would artificially increase $k_\perp$. Thus, although the $p_\perp$ sharpening in Fig. 16 is encouraging, further work is needed to understand both biases in selection of jet vector, loss of trigger jet and gain of beam/target jet particles.

D. Make-up of Trigger Jet (E260, Refs. 10, 11)

Even the E395 calorimeter finds it hard to unambiguously resolve the calorimeter signals into individual particles. An important advantage of the E260 setup is that although neutrals are hard to resolve, it is very easy to find out about the charged particle component of the jet. In Fig. 17,

we plot the z distributions (i.e., fraction of jet transverse momentum) for the charged particles in the jet. As shown in the figure, there are striking similarities with the corresponding distributions seen in lepton processes. Although the data in Fig. 17 are summed over all jet $p_\perp$, it is shown in Ref. 10 that the z distribution is essentially independent of $p_\perp$. This scaling is, of course, expected in constituent models and taken in conjunction with the similar shape to lepton data, seems to be impressive support not only for the hard scattering models but also for the identification of the constituents with the quarks present in lepton processes.

Although the data are, as in C, encouraging, I believe that strong conclusions are premature. First, the exact shape of the z distribution seen in Fig. 17 is sensitive to the calorimeter acceptance. For instance, as we remarked in C, low z high $k_\perp$ particles are lost and less than 50% of the particles from a SPEAR jet for $z < 0.2$ would hit the E260 calorimeter. The agreement, even for $z < 0.2$, of the data with the SPEAR results, implies that lost jet members are roughly compensated by additional particles from the beam jet. This cancellation does mean that the jet estimates in E260 do not need serious acceptance correction but shows that precise agreement with lepton processes is somewhat accidental. This is illustrated in Fig. 18, where we compare the z distribution from Fig. 17 with data from the same group but in a later run[11] with the calorimeter placed at larger angles so as to be centered at 90° in the cms. The newer data are clearly flatter than the older values and in much poorer agreement with the lepton values. We currently believe that this just means that acceptance of the calorimeter is poorer in its 90° position and so the loss of low z particles is accentuated and not compensated fully by beam/target jet members as in Fig. 17.

We would now like to discuss another problem that was suggested theoretically by Field and Feynman[17] and experimentally by E395[12]. Thus, in e^+e^- collisions with beam energy E, one produces a quark-antiquark pair each with this energy E. These then fragment into particles with energy E_i and momentum fraction z_i. Here one defines $z_i = p_{z_i}/E$, where p_{z_i} is momentum component of particle along $q\bar{q}$ direction. Summing over all the fragments of one of the quarks, one has, averaged over events,

$$\langle \sum_i E_i \rangle = E$$

$$\langle \sum_i (E_i - p_{z_i}) \rangle > 0$$

i.e.,

$$z_i = p_{z_i}/E \tag{1}$$

$$= p_{z_i}/\sum_j E_j \quad \text{on average} \tag{2}$$

$$< p_{z_i}/\sum_j p_{z_j} \quad \text{on average} \tag{3}$$

Now (3) is the definition used in the hadron analysis, Fig. 17, as $\sum_i p_{z_i}$ is just the $p_\perp$ of jet. Unfortunately,

$$\Delta = \sum_i (E_i - p_{z_i}) \tag{4}$$

is large - as can readily be estimated[17,30]

$$\langle \Delta \rangle = \int_0^\infty (E - p_z) \frac{1}{\sigma} d\sigma/dy \, dy$$

$$= \langle m_T \rangle \int_0^\infty e^{-y} \frac{1}{\sigma} d\sigma/dy \, dy \, , \quad m_T = \sqrt{m^2 + p_\perp^2}$$

$\sim \langle m_T \rangle$ x density of particles per unit rapidity at y=0 (in quark fragmentation)

$\sim$1 GeV/c .

Thus the denominator in correct definition of z, namely (1), is roughly 1 GeV/c larger than value used by E260. Correspondingly, the z distribution should be sharpened so that $\langle z \rangle$ decreases by $\sim$ 25%. (Note for $z \sim 1$ the distribution is not changed much as the particles with large z correspond to (unusual) quark fragmentations where $E \sim \Sigma\, p_z$.)

Unfortunately, the masses and, hence, energies of the particles are not known experimentally. Further, $\sum_i (E_i - p_{z_i})$ is dominated by the contribution of low z particles where it is essentially impossible to distinguish trigger jet members from beam and target jet fragments. Thus, the calculation of Δ is hard to do on an event by event basis. We can look at this in Monte Carlo simulations but currently we can only view Fig. 17 as qualitative agreement between jets in lepton and hadron processes. In particular, the current data would clearly allow substantial contribution from gluon jets which would be expected to fragment with a sharper z distribution than quarks. Until E260 has completed its Monte Carlo studies (using the model of Ref. 17), I don't know how quantitative it will be possible to make the lepton hadron comparison. I fear it may be impossible to do any more than qualitative comparisons until we get hadron jets of substantially higher $p_\perp$.

E. Away Side Distributions (E260, Refs. 10, 11)

Perhaps the firmest results in hadronic jet physics are the comparison of jet and single particle triggers shown in Figs. 19 and 20. This only uses particles outside the jet and so is insensitive to the ambiguities that have plagued the previous sections. In Fig. 19, we compare the away side distributions for jet and single particle triggers. These are plotted in terms of $z_J = p_{x'}/p_\perp^{jet}$ for the jet triggers while for the single

particles, we use "z_J" = $-p_{x'}/(p_\perp^{s.p.} + 0.85)$. The 0.85 factor is just $\langle z_{trigger} \rangle$ in the model described in Section II; historically, it resulted from a telephone call from me to Rick Field on the night before a defense and plea for further running of E260 at Fermilab. (At a time when we didn't really believe in jets and we were searching for some hint that our jet data were meaningful and not a random collection of junk. We did get additional running but maybe the 0.85 wasn't critical for this.) In any case, the 0.85 is not only theoretically expected but also consistent with the additional $p_\perp$ seen in the E260 calorimeter for single particle triggers. Furthermore, this factor brings the single particle and jet data into striking agreement in Fig. 19. This I consider very strong evidence that jets and single particles are governed by similar dynamics at high $p_\perp$.

The fact that the z_J distributions on the away side are about a factor of 3 below the trigger side again indicates the need for internal motion of constituents to ensure $p_\perp$(trigger) > $p_\perp$(away). The quantitative comparison of the theory with experiment will be confused by the argument in D that I should define z by dividing by jet energy not $p_\perp$. In fact, the alert reader will notice that the fact that the jets should be compared with single particles using the jet energy, not $p_\perp$, confuses the theoretical argument for the $\langle z_{trigger} \rangle$ = 0.85 factor. Thus, the jet energy is about 20% higher than its $p_\perp$ and one naively predicts a net factor 0.85 x 1.2 ~ 1 for scaling single particle distributions! This would destroy agreement between the two triggers. I don't fully understand the resolution of this problem; one point, worth noting, is that because the jet energy spectrum is rapidly falling, a plot versus $p_\perp^{jet}$ will be dominated by jets which have much lower values of $\sum_i (E_i - p_{z_i})$ than the unbiased value $\Delta \sim 1$ GeV[31].

Fig. 19 also shows a small violation of scaling of the z_J distributions with trigger $p_\perp$. This comes from Ref. 10; the better statistics available from the new E260 data (Ref. 11) should allow a definitive study and comparison with the single particle trend shown in Figs. 4, 6 and 7.

In Fig. 20, we compare the gross structure of charged particles in single particle and jet triggers. We define five kinematic regions; T_o is all particles into trigger calorimeter. The remaining particles are divided by a cut on $p_{x'}$, ($p_{x'}$ > 0 is trigger T and $p_{x'}$ < 0 away side A) and a cut on rapidity > and < 1. Both the multiplicity and momenta are similar for single particles and jets. It is quite interesting that both triggers see roughly the same number of particles outside the calorimeter on the trigger side; one might have expected that the jet trigger would have biased you to events in which trigger side particles were dragged into calorimeter with the rest of trigger side being relatively unpopulated. This does not seem to be the case. Further discussion of the data in Fig. 20 can be found in Ref. 10.

F. Internal Motion of Constituents (E395, Ref. 12)

There is now ample evidence for the internal motion of constituents inside the hadron. We discussed this in Section II theoretically and it was indicated by the low values of the away side z_p, $p_\perp^{jet}$, or z_J distributions in Sections IV, VB, and VE. Also, the asymmetry in population of the forward regions A_{II} and T_{II} in Fig. 20 can be interpreted in terms of this motion. Further evidence comes from the E395 data shown in Fig. 21. These results come from a trigger on the sum of the transverse momenta in the left plus right calorimeter. Naively, the distribution in $p_\perp$(left) - $p_\perp$(right) for fixed sum directly reflects internal transverse momenta of

partons. We see from Fig. 21(a) that the difference has quite a broad distribution and E395 calculates the root mean internal momentum $\langle k_T \rangle$ as the standard deviation of the distribution in $p_\perp$(left) - $p_\perp$(right). The resultant $\langle k_T \rangle$, divided by $\sqrt{2}$, is shown in Fig. 21(b). The mean values are very large - if anything bigger than the value $\langle k_T \rangle \sim 800$ MeV/c suggested by the dimuon experiments[27]. Obviously, this is not a firm conclusion because the derivation of $\langle k_T \rangle$ is only correct if the calorimeters see all particles in trigger/away jet and have no contamination from stray particles in beam and target jet. Any such loss or gain of particles will probably tend to increase the width of the $p_\perp$(left) - $p_\perp$(right) distribution, and so the results in Fig. 21(b) should perhaps be viewed as an upper bound on $\langle k_T \rangle$.

G. The Jet Cross-Section (E236, 260, 395, Refs. 9-12)

Results from E260 and E395 on the jet cross-section are shown in Figs. 22 and 23 for 200 and 400 GeV/c beams, respectively. The E260 results correspond to a Beryllium target but a preliminary analysis[11] of data on hydrogen shows there are no problems using nuclear target data. I do not show the E260 proton target cross-sections because of the acceptance problems indicated in Fig. 18. Further, the Be analysis used a better treatment of the neutral component of jet than that in Ref. 11. A striking feature of Figs. 22 and 23 is that not only is the jet cross-section large but that both experiments get about the same ratio (100-200) compared to the single particle cross-section. (The actual values of the jet cross section in Figs. 22 and 23 differ by almost an order of magnitude at high $p_\perp$ but this is just the ratio of single particle cross-sections for the two different beam energies.) A universal ratio of jet to single

particle cross-section is the natural prediction of any model where jets and single particles come from the fragmentation of (the same) constituents. The agreement on this ratio at the two different energies is indirect evidence that jets have a similar (e.g., $p_\perp^{-8}$, not $p_\perp^{-4}$) $p_\perp$ dependence (at fixed $x_\perp$) to the single particles. It is not very conclusive as the two experiments have very different calorimeters and it is not clear that corrections for the different acceptances wouldn't alter the comparison between the two energies. We should soon have comparisons of jet cross-sections at different energies from the same experiment. In fact, a preliminary analysis of E236 data at 100 and 340 GeV/c suggests a slower fall off with $p_\perp$ for the jets compared to the single particles[9].

In Fig. 22, we show that the predictions of the FFF quark scattering model[32] agree nicely with E260; this model will also agree with the E395 data shown in Fig. 23 (as it predicts a universal ratio to the single particles). Unfortunately, I now believe that the agreement in Figs. 22 and 23 is fortuitous and that the measured jet cross-sections are substantially larger than the FFF predictions. This is a consequence of the problem mentioned in Section VD, that one should really compare the theory with the jet energy and not the jet $p_\perp$ distribution. A preliminary estimate, based on the model of Ref. 17, suggests that the energy distribution will be about a factor of five larger than the $p_\perp$ one[31]. This factor then represents a discrepancy between FFF and the measured jet cross-sections. One can and should investigate the differences between the energy and $p_\perp$ spectrums experimentally. Unfortunately, as the difference between E and $p_\perp$ comes entirely from the ambiguous low $p_\perp$ particles, I fear the results will be inconclusive.

In Figs. 24 and 25, we show two results from E260 that only involve ratios and so are insensitive to the above problems. First in Fig. 24, we compare π^- and proton induced cross-sections. There is a clear trend with a ratio proton/π^- of ~ 1.5 at low $p_\perp$ decreasing to around 0.6 above $p_\perp$ = 5 GeV/c. As the figure shows, this is in striking agreement with the single particle π^o beam ratio from Ref. 2. (The $p_\perp$ scale for π^o's has been increased by 0.85 as in Section E.) The agreement with the FFF prediction, shown in Fig. 24, is partly fake as the theory was adjusted to give agreement with the π^o data. E395 reports a similar π/p ratio to E260 but it is currently of less statistical significance[12]. Finally in Fig. 25, we show the A dependence extracted from a comparison of hydrogen and aluminum targets[11]. Again, there is nice qualitative agreement with the single particle data which we have already discussed in Section III. These observations strengthen the comparison between the dynamics of single particle and jet physics. The similar dynamics argues against the (commonly held) ideas that hadron jet phenomena are either trivially obvious or just the study of "random" collections of particles.

H. Conclusions on Jet Triggers

In the preceding sections, I have tried to show that there is mounting evidence that there is a large cross-section for hadronic jet production where the jets have (all) the properties expected from constituent fragmentation models. I have also tried to indicate the many uncertainties in the current analysis. Nearly all the problems are connected with the low momentum particles in the jet. These problems are, unfortunately, probably insoluble. There is, in principle, no valid way to say if a particle at low z, i.e., in rapidity plateau of quark fragmentation,

belongs to trigger, beam, target or away side jet. For instance, the results will depend theoretically on the frame (e.g., beam target cms or hole[18]) used for the constituent decay. At the moment, the only safe way I can see to get a reliable analysis is to define a "jet" only using particles with a transverse momentum greater than a certain cut off (500 MeV/c, say, for the current 5 GeV/c jets). This "jet" will certainly have a lower cross-section than the "true" value; however, it is a lower value that can be reliably defined experimentally and calculated theoretically. For these reduced jets, there should be little trouble in comparing the results from calorimeters of different acceptances. Conversely, as long as jets are defined as all particles entering a particular calorimeter, there are bound to be differences between the results of the different experiments. It is my current impression (for the calorimeter sizes in Table I) that these differences are all connected with the ambiguous low z particle, and hence, not important. (Although if you wish to compare a particular calorimeter cross-section with a theoretical model, one must ask if one has an excess or deficit of low z particles.) Experimentally, one must aim to design experiments that are sensitive to the highest possible $p_\perp$; thereby, one minimizes the low z uncertainty and will even see events that are clearly jet-like on an event by event basis. Further, one becomes sensitive at high $p_\perp$ (10-15 GeV/c) to the possible $p_\perp^{-4}$ term in the jet production coming from the QCD gluon exchange in quark quark scattering[20,33].

In spite of my reservations expressed above, past and future jet experiments have and will teach us a lot about high $p_\perp$ dynamics; these lessons should be a part of any model for particle production at high $p_\perp$.

Acknowledgments

I would like to thank Rick Field for many important discussions. Kar Yung did most of the work in preparing the new E260 data. I am grateful to the experimentalists who contributed the many interesting and new pieces of data to this talk.

References

1) J. W. Cronin et al., Phys. Rev. D11, 3105 (1975) and Phys. Rev. Letters 38, 112, 115 (1977).

2) G. Donaldson et al., Phys. Rev. Letters 36, 1110 (1976).

3) P. Darriulat, in Proceedings of the Eighteenth International Conference on High Energy Physics, Tbilisi, U.S.S.R. (1976), edited by N. N. Bogolubov et al.

4) H. Boggild, Invited talk at VIIIth Symposium on Multiparticle Dynamics, Kaysersberg, France (1977).

5) H. Frisch, in BNL Report No. BNL-50598, edited by H. Gordon and R. F. Peierls, Proceedings of the American Physical Society Meeting, Division of Particles and Fields, Upton, New York (1976), (unpublished).

6) C. W. Akerlof et al., Phys. Rev. Letters 39, 861 (1977).

7) R. L. McCarthy et al., "Atomic Number Dependence of the Production Cross-Sections for Massive Dihadron States," preprint (1977). (E494).

8) R. J. Engelmann, private communication (1977). (E494).

9) K. Young, private communication (1977). (E236).

10) C. Bromberg et al., Phys. Rev. Letters 38, 1447 (1977); C. Bromberg et al., "Production of Jets and Single Particles at High $p_\perp$ in 200 GeV Hadron Beryllium Collisions," preprint (1977). (E260, Beryllium target).

11) C. Bromberg et al., "Comparison of Hadronic Jets Produced by π^- and p Beams on Hydrogen and Aluminum Targets," preprint (1977) and further analysis. (E260, H_2 and Al Target).

12) L. Cormell et al., "Evidence for Jets, and for Correlated Jets, in High $p_\perp$ Events," preprint (1977). (E395).

13) S. M. Berman, J. D. Bjorken and J. B. Kogut, Phys. Rev. D4, 3388 (1971); J. D. Bjorken, Lectures delivered at the SLAC Summer Institute on Particle Physics, July 1975.

14) S. D. Ellis and M. B. Kislinger, Phys. Rev. D9, 2027 (1974).

15) S. D. Ellis, M. Jacob and P. V. Landshoff, Nucl. Phys. B108, 93 (1976) and S. D. Ellis and P. V. Landshoff, Nucl. Phys. B113, 395 (1976).

16) R. D. Field and R. P. Feynman, Phys. Rev. D15, 2590 (1977); R. P. Feynman, R. D. Field and G. C. Fox, "Correlations Among Particles and Jets Produced with Large Transverse Momenta," preprint (1977).

17) R. D. Field and R. P. Feynman, "A Parameterization of the Properties of Quark Jets," preprint (1977).

18) G. C. Fox in BNL report cited in Ref. 5.

19) CCHK Collaboration, "Observation of Jet Structure in High $p_\perp$ Events at the ISR and the Importance of Parton Transverse Momentum," preprint, CERN/EP/PHYS 77-10 Rev. (1977).

20) R. D. Field and R. P. Feynman, private communication (1977).

21) D. Bintinger et al., Phys. Rev. Letters 37, 732 (1976).

22) P. Darriulat et al., Nucl. Phys. B107, 429 (1976).

23) D. C. Hom et al., Phys. Rev. Letters 37, 1374 (1977).

24) R. Moller, "Jets and Quantum Numbers in High $p_\perp$ Hadronic Reactions at the CERN-ISR," talk at Moriond Conference (1977).

25) F. W. Busser et al., Nucl. Phys. B106, 1 (1976).

26) S. J. Brodsky, R. Blankenbecler and J. F. Gunion, "Large Transverse Momentum Processes and the Constituent Interchange Model," SLAC preprint (1977).

27) S. W. Herb et al., Phys. Rev. Letters 39, 252 (1977).

28) G. Hanson et al., Phys. Rev. Letters 35, 1609 (1975).

29) J. C. VanderVelde, "Neutrino Interactions in the 15-Foot Bubble Chamber and Search for Charmed Particles," preprint and invited talk at Moriond Conference (1977).

30) R. P. Feynman, "Photon-Hadron Interactions," (Benjamin, Reading, Mass., 1972).

31) R. D. Field, private communication.

32) R. D. Field, "Implications of the Recent Large $p_\perp$ Jet Trigger Data from Fermilab," preprint and invited talk at the Moriond Conference (1976).

33) R. Cutler and D. Sivers, Phys. Rev. D16, 679 (1977); B. L. Combridge, J. Kripfganz and J. Ranft, Phys. Letters 70B, 234 (1977).

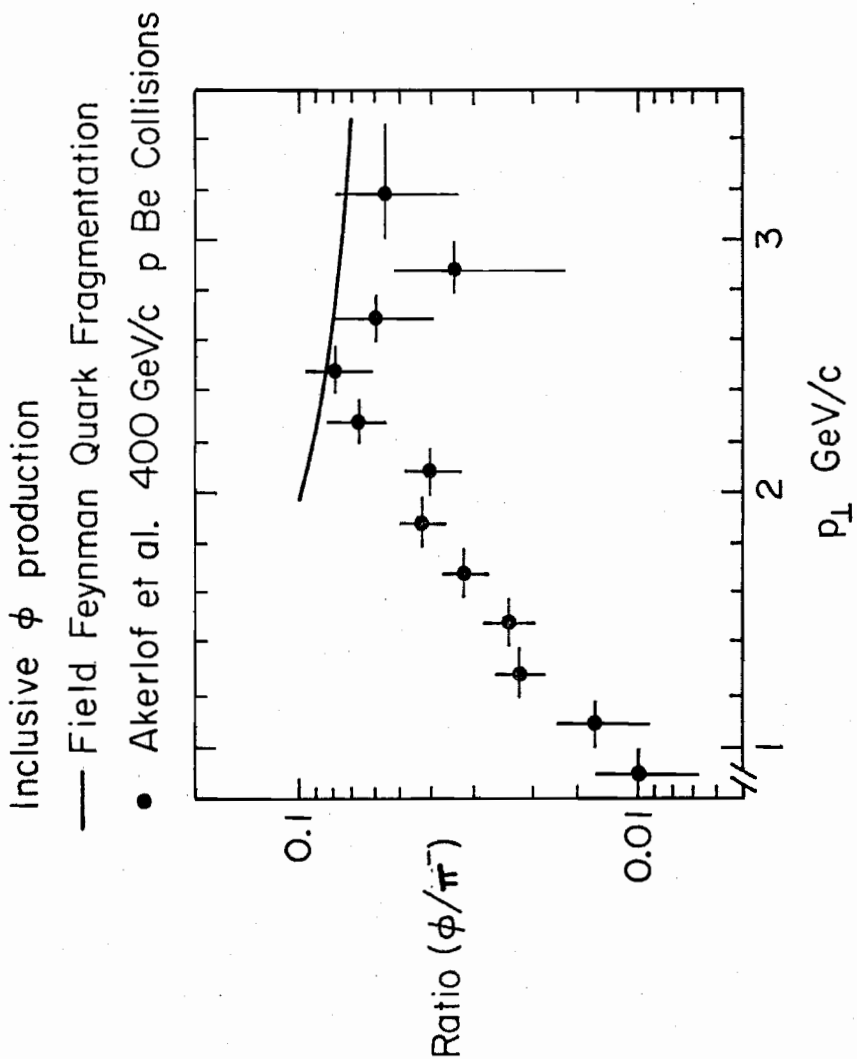

Figure 1: The ratio of ϕ to π^- inclusive production in 400 GeV/c proton Beryllium collisions as a function of $p_\perp$. The data are from Ref. 6 and the theoretical prediction from Ref. 17.

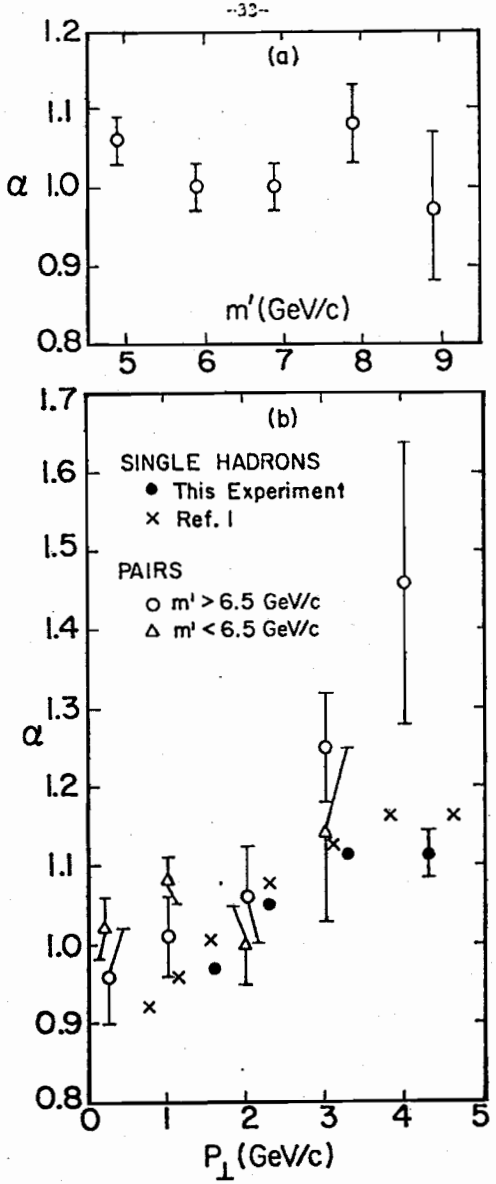

Figure 2: The power α of the A dependence of the invariant dihadron production cross section from E494[7]. α is plotted (a) as a function of dihadron mass m' for all $p_\perp$ and (b) a function of dihadron $p_\perp$ for m' < and > 6.5 GeV. Comparison is made to the single particle A dependence both from E494 and Chicago-Princeton (Ref. 1).

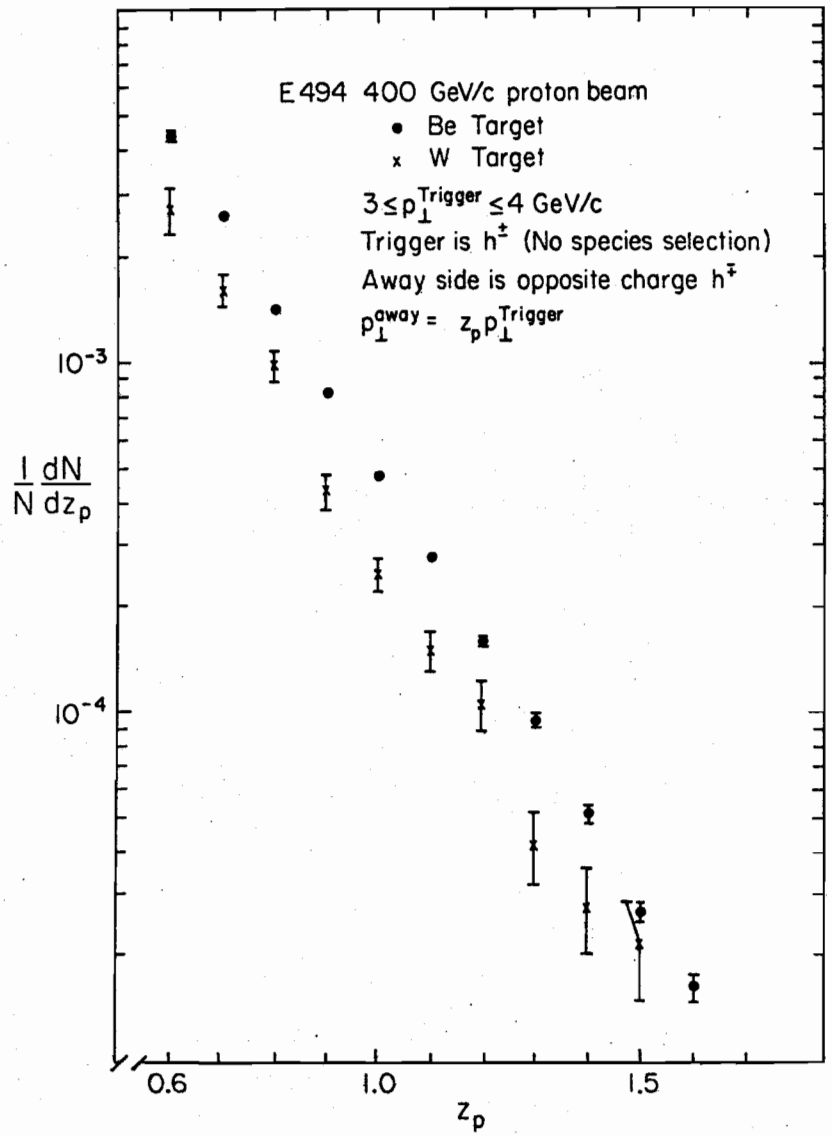

Figure 3: Comparison of the z_p (x_e) distributions for Beryllium and Tungsten targets from E494[8)]. No correction has been made for acceptance of apparatus.

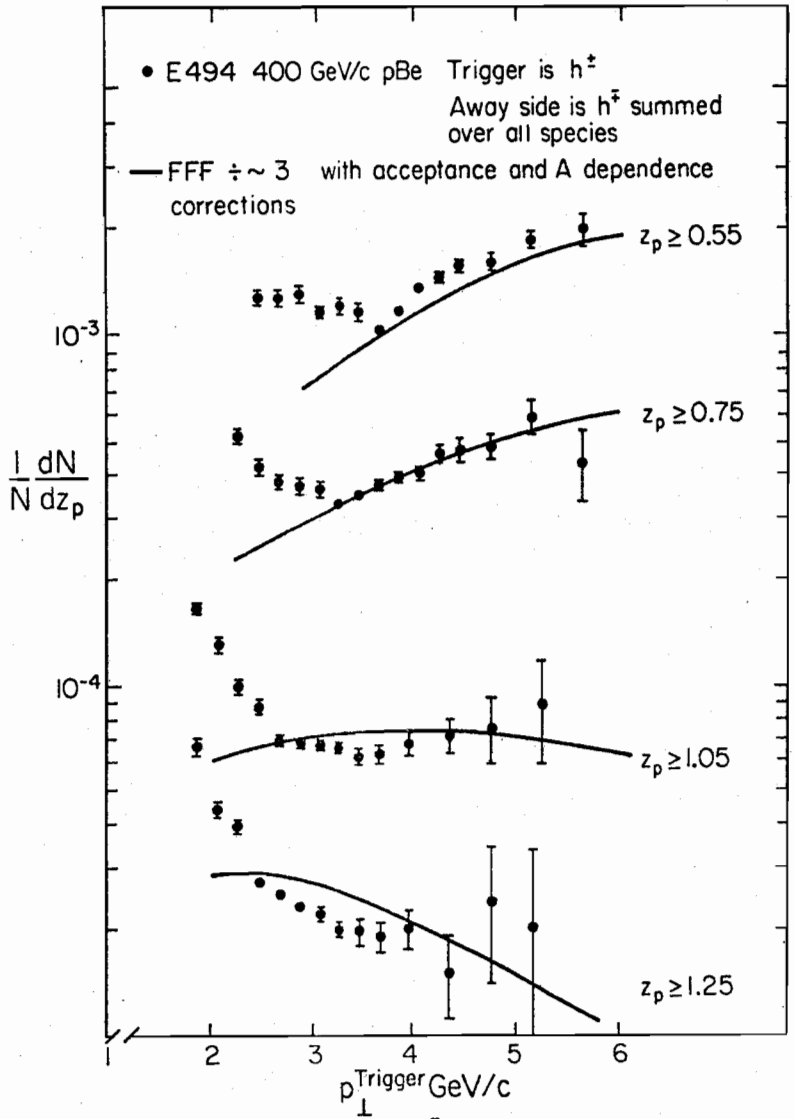

Figure 4: Trigger $p_\perp$ dependence of $1/N \int_{z_p}^{\infty} dN/dz_p' \, dz_p'$ for different z_p cuts[8)]. The predictions[16)] of FFF have been calculated including the apparatus acceptance and divided by a factor of ~ 2.5 to get the approximate trend of the data. This calculation includes an estimate of the A dependence. ($1/N \, dN/dz_p$ for Be is roughly 2/3 of that for a proton target.)

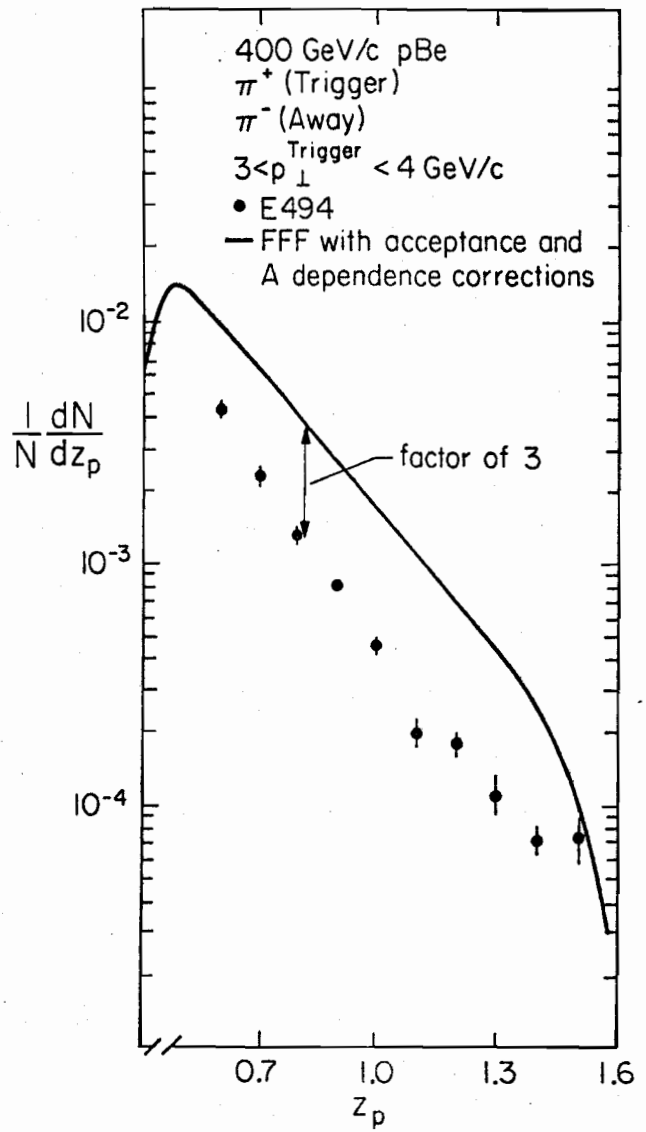

Figure 5: z_p distribution for a π^+ trigger and π^- on the away side averaged over a trigger $p_\perp$ range of 3 to 4 GeV/c. The data are from E494[8] and the FFF theory[16] has A dependence and apparatus acceptance corrections and is absolutely normalized.

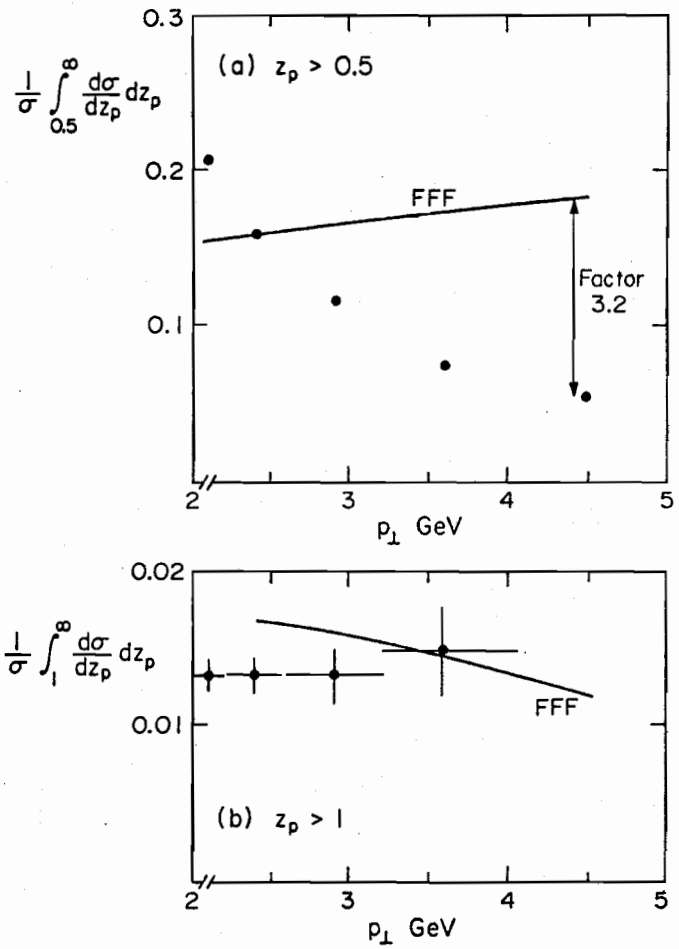

CCHK All charged particles on away side

$|\phi-(180-\phi_{trigger})| \leq 40°$

Average of 20°, 45° triggers

$\sqrt{s}$ = 53 GeV

Figure 6: z_p distributions versus trigger $p_\perp$ from CCHK, Ref. 19, compared with the absolutely normalized FFF calculation (Ref. 16).

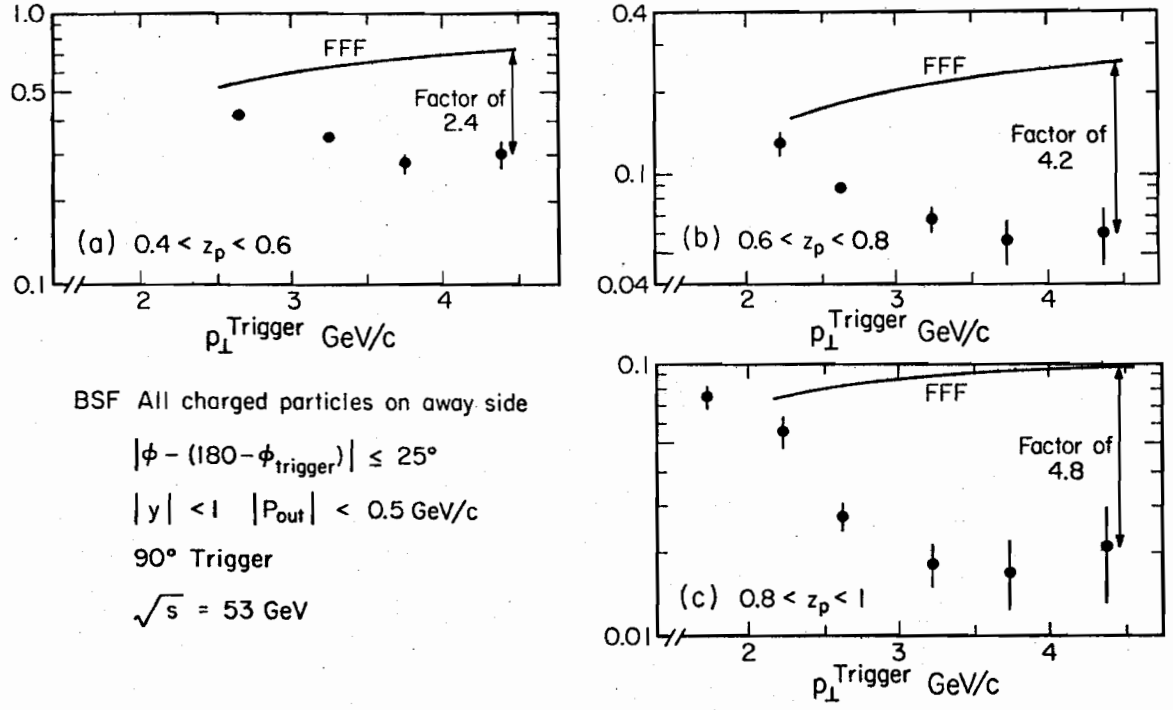

Figure 7: z_p distributions versus trigger $p_\perp$ from BFS, Ref. 4, compared with the absolutely normalized FFF calculation (Ref. 16).

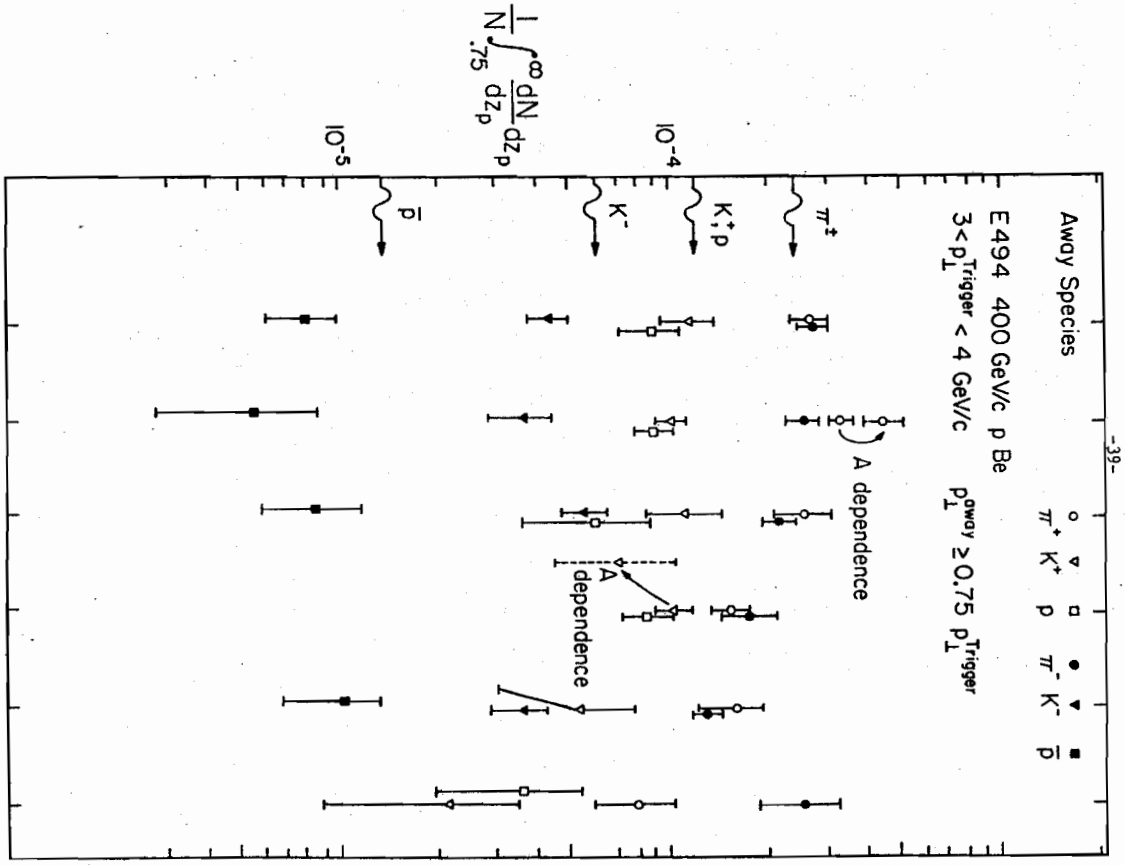

Figure 8: $\frac{1}{N}\int_{0.75}^{\infty} \frac{dN}{dz_p} dz_p$ for 6 trigger and 6 away side species for the trigger $p_\perp$ cut of 3 to 4 GeV/c. The data come from E494 and the wavy lines at the side indicate the rate you would expect if the away side yield had the same rate as the trigger side (only the relative values of the wavy lines are significant, the absolute level is adjusted by eye). The data have not been corrected for the A dependence; the typical magnitude of this is shown by two dashed data points. Not all the 36 possible data points are plotted due to limited statistics on the same sign charge configurations.

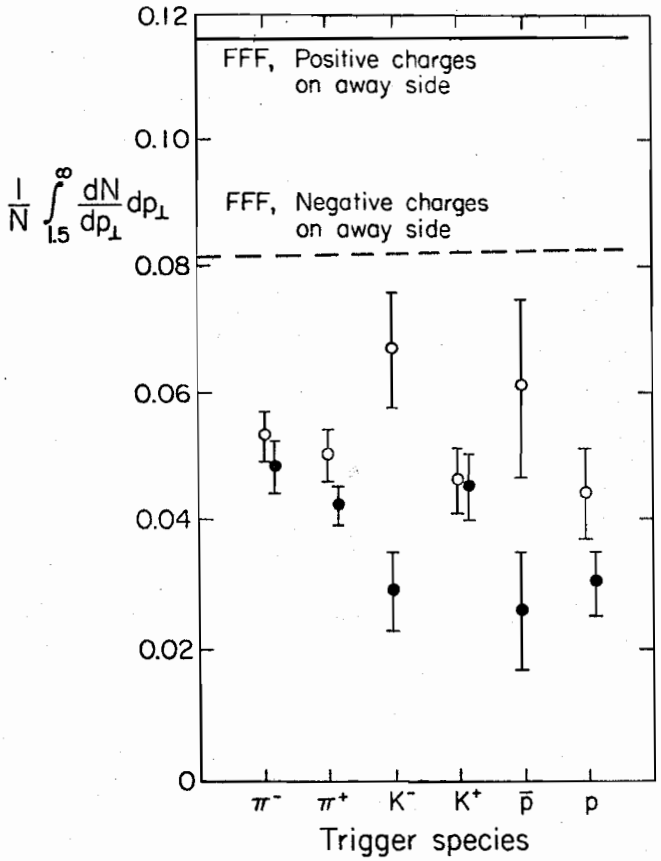

BFS Experiment
ISR R413
$3 \leq p_\perp^{trigger} \leq 4.5$ GeV/c at 90°
$\sqrt{s}$ = 53 GeV
o Positives on away side
● Negatives on away side
$p_\perp$ (away) > 1.5 GeV/c
|Rapidity (away)| < 1
Away side theory (FFF) independent of trigger species

Figure 9: Data on the number of away side particles of different charge as a function of the trigger species. The away side $p_\perp$ is > 1.5 GeV/c and the trigger side $p_\perp$ between 3 and 4.5 GeV/c. The data are from Ref. 4 and the theory which is, as always on the away side, too large is from Ref. 16. The theory predicts results for the different meson trigger species that are approximately equal (the differences ~ 2%).

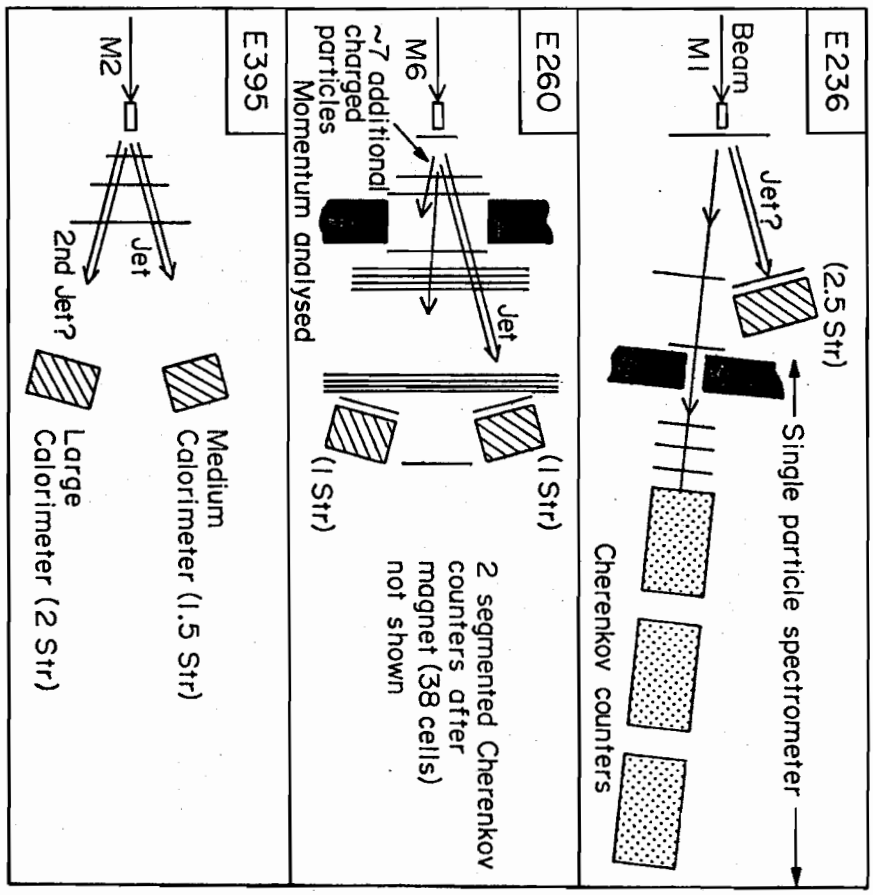

Figure 10: Schematic representations of the three Fermilab jet experiments compared in Table I.

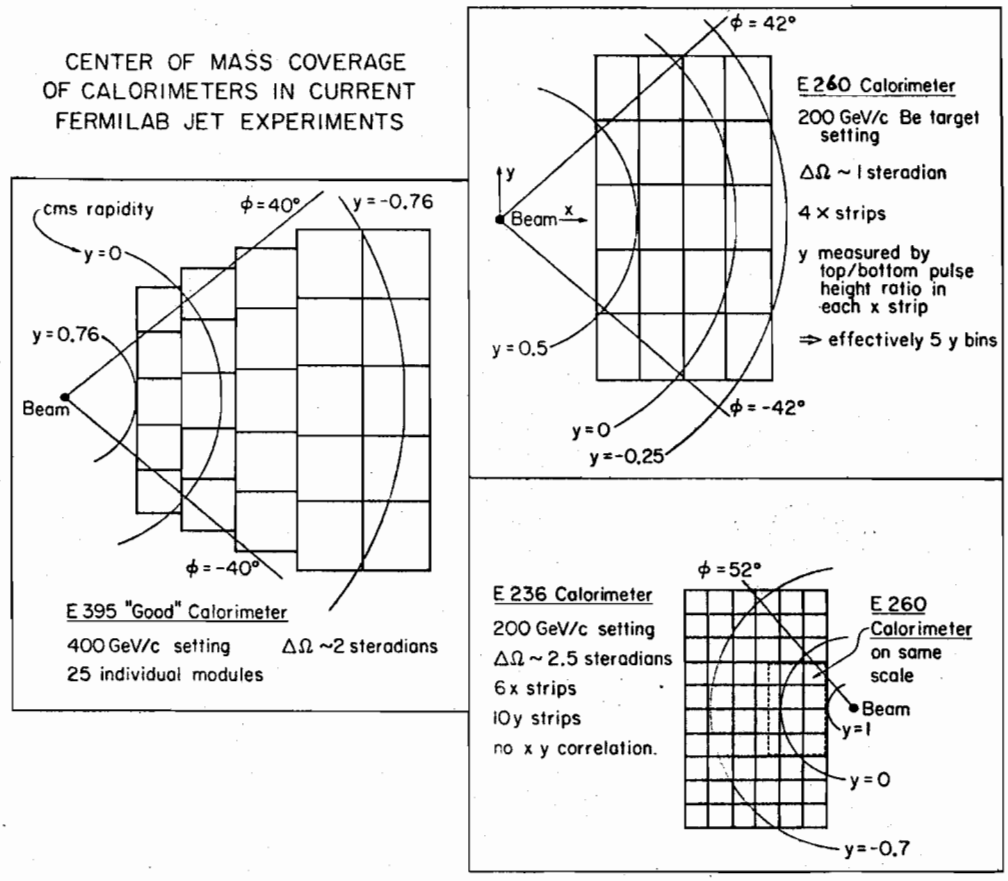

Figure 11: Center of mass coverage (in terms of azimuth ϕ and rapidity y) for the three Fermilab jet experiments compared in Table I. E236 and 260 are shown for 200 GeV/c, E395 for 400 GeV/c. Note that the different coverages reflect more different distances from the target than different calorimeter sizes. For E260, the size of the y bins is set to three times measurement resolution.

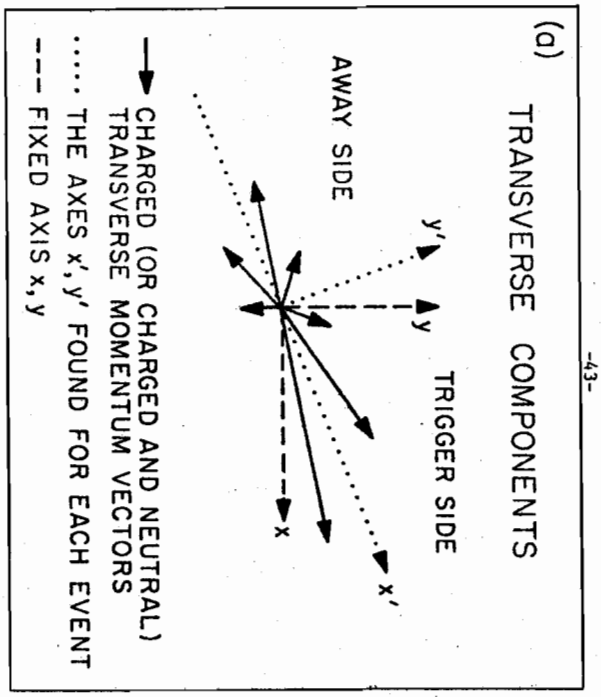

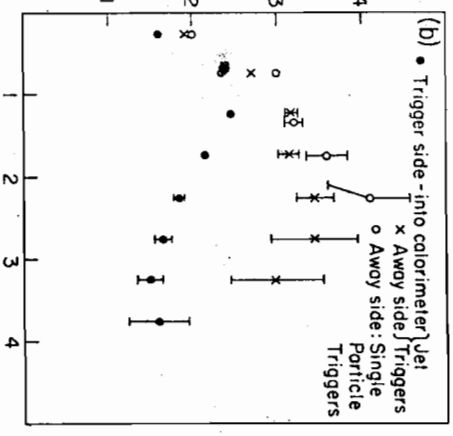

Figure 12: (a) Illustration of transverse momentum vectors (solid lines) of a typical event in E260 and the axes x',y' found on an event by event basis so that $\Sigma\, p_{y'}^2$, is minimized. x,y are the fixed axes. (b) Variation of $\langle p_{y'} \rangle$ with particle $p_{x'}$ for jet and single particle triggers. These data are averaged over $p_\perp^{jet}$ or $p_\perp^{s.p.} \geq 0.85$ greater than 2.6 GeV/c. This figure comes from E260 (Ref. 10).

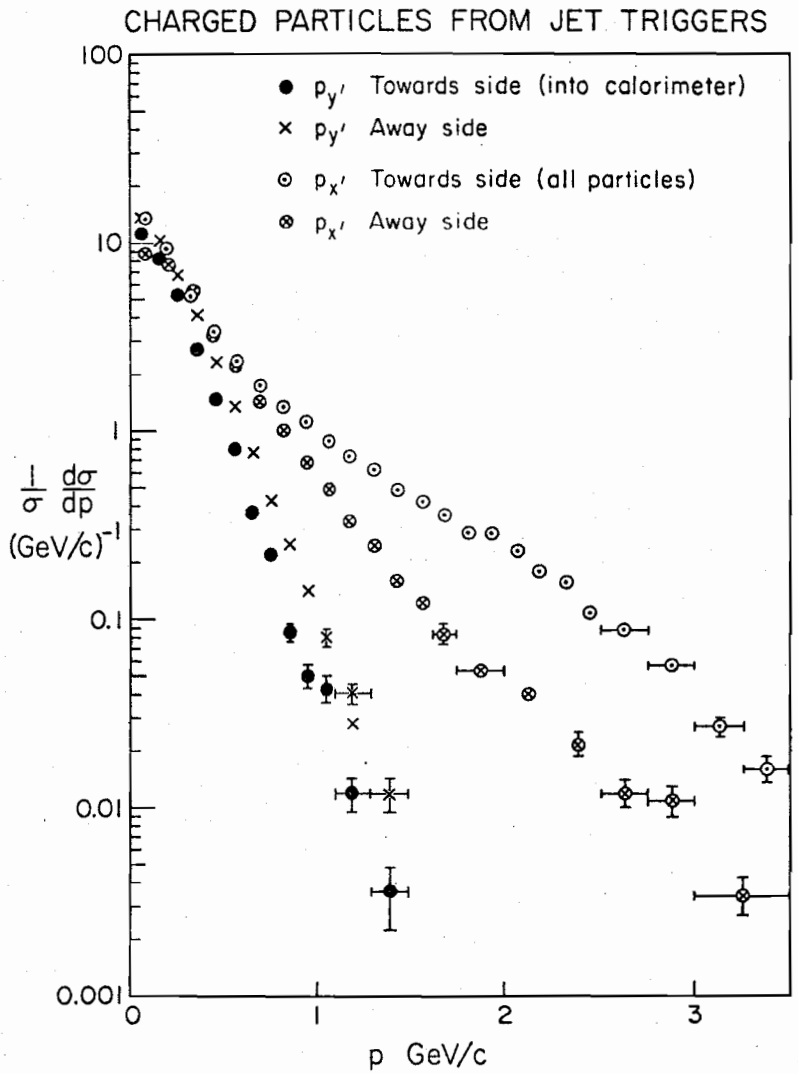

Figure 13: Distributions in $p_{x'}$ and $p_{y'}$ for jet data with $p_\perp^{jet} > 2.6$ GeV/c (E260, Ref. 10).

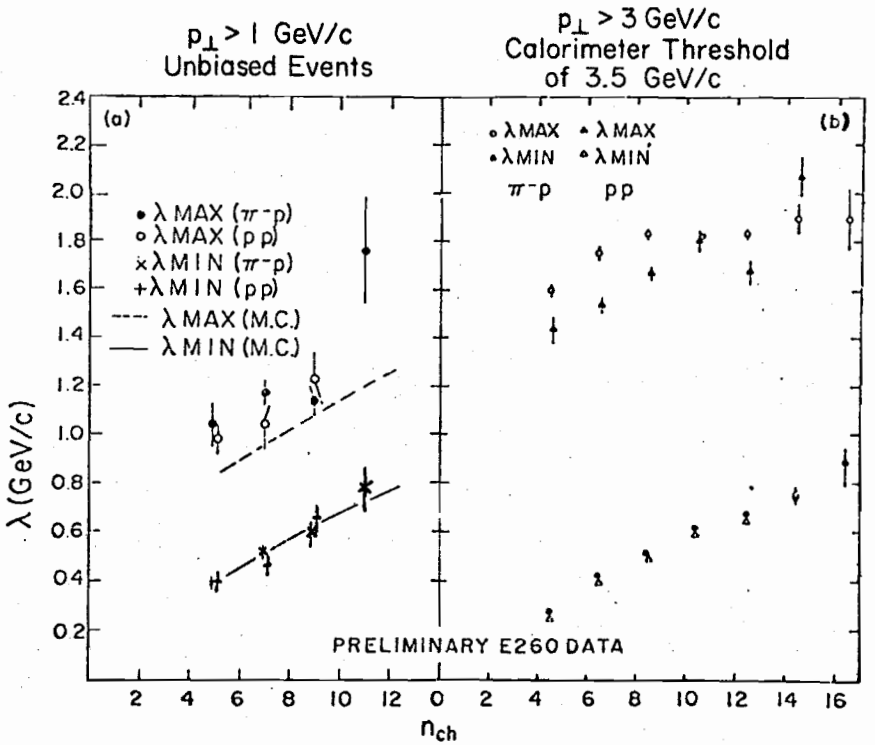

Figure 14: Variation of λ_{min} and λ_{max} (defined in Section VA of the text) with charged multiplicity. Data (Ref. 11) are shown for both π^-p and pp scattering. In (a), the data come from a simple interaction trigger which did not involve the calorimeter and is selected offline to have $p_\perp^{jet} > 1$ GeV/c in calorimeter. It is compared with a Monte Carlo calculation assuming uncorrelated particle production generated according to observed single particle $p_\perp$ distribution (E260, Ref. 10). (b) Data from jet triggers with $p_\perp^{jet} > 3$ GeV/c.

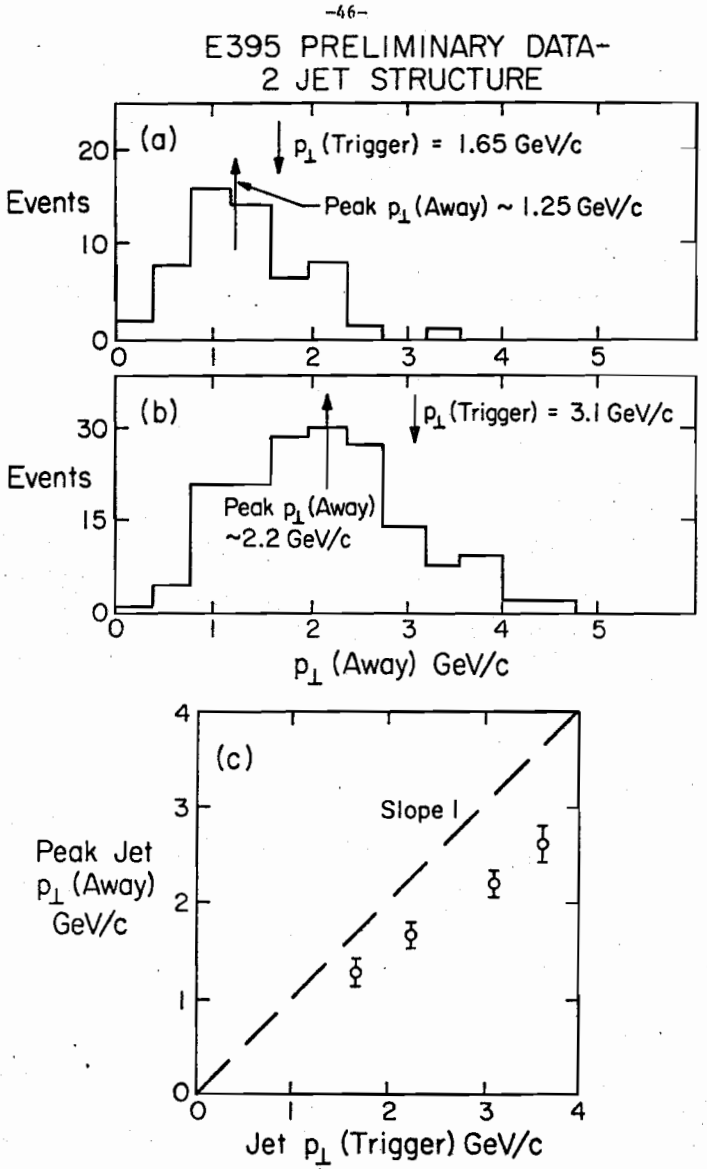

Figure 15: (a), (b) The distribution of jet $p_\perp$ in the good "right" calorimeter for two different trigger jet $p_\perp$'s in the "left" calorimeter. Cuts have been made that both trigger and away jets have vectors that lie in middle 0.1 str. of each calorimeter.
(c) Plot of peak in away side jet $p_\perp$ distribution versus trigger $p_\perp$ (Ref. 12, E395).

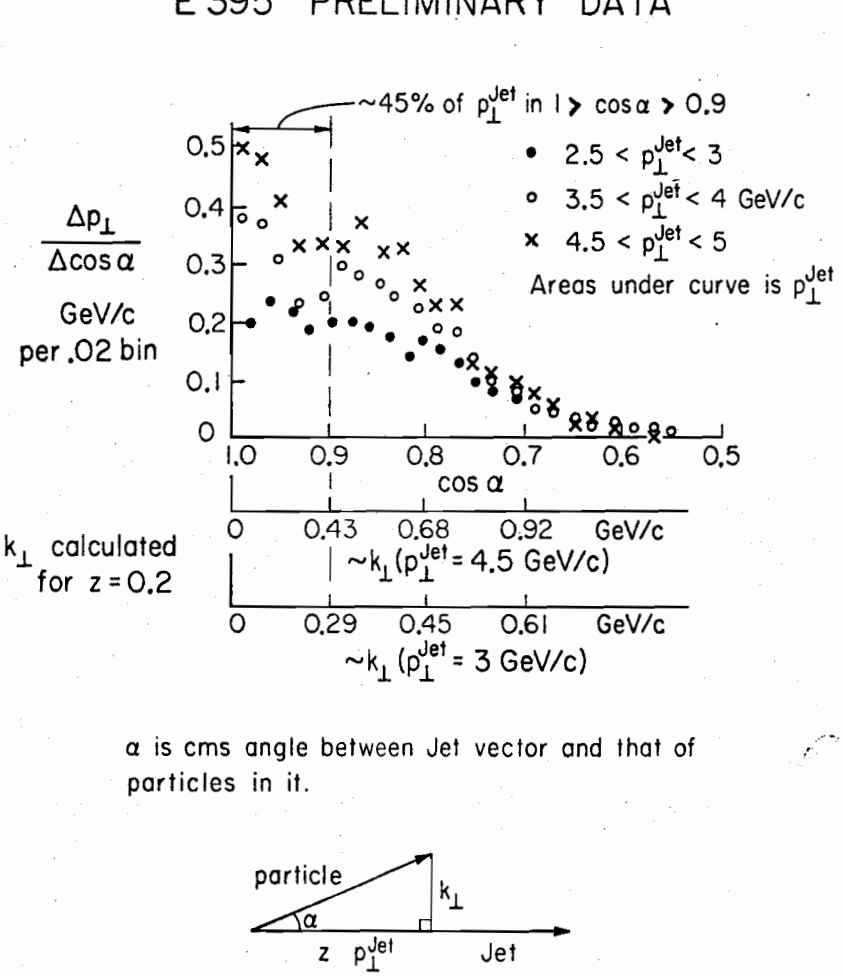

α is cms angle between Jet vector and that of particles in it.

Figure 16: Distributions in the cms angle α between jet vector and individual particles within the jet. The data (Ref. 12, E395) are normalized so that area is proportional to jet $p_\perp$ and shown for three different trigger $p_\perp$ bands (Ref. 12, E395). I show the equivalent $k_\perp$ scale for two $p_\perp$ values. This uses the $\langle z \rangle$ = 0.2 measured in E260; probably E395 is somewhat lower than this due to their better low z acceptance.

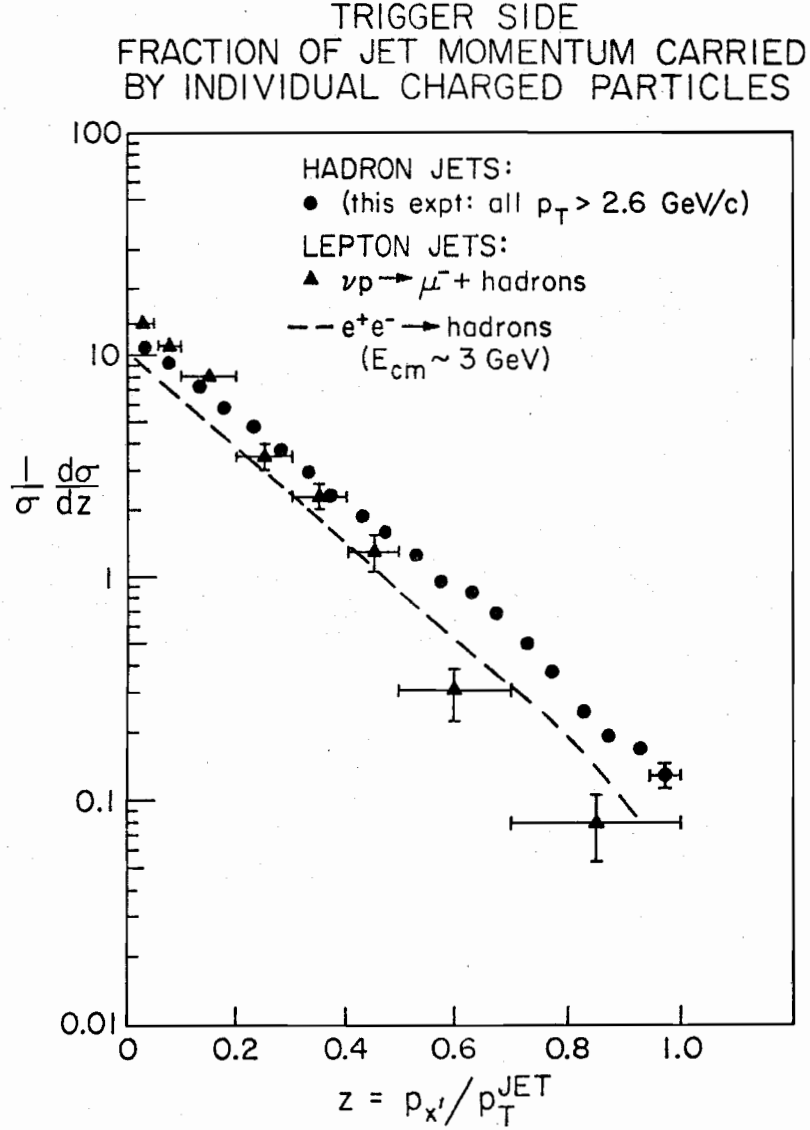

Figure 17: Distribution of momentum fraction $z = p_{x'}/p_1^{jet}$ for the charged particles in the trigger jet. The data from E260 (Ref. 10) are taken from the early Be target run with the calorimeter centered at cms rapidity 0.25 (the configuration shown in Fig. 11). Also shown are the analogous distributions in lepton processes; e^+e^- collisions (Ref. 28) and νp interactions (Ref. 29).

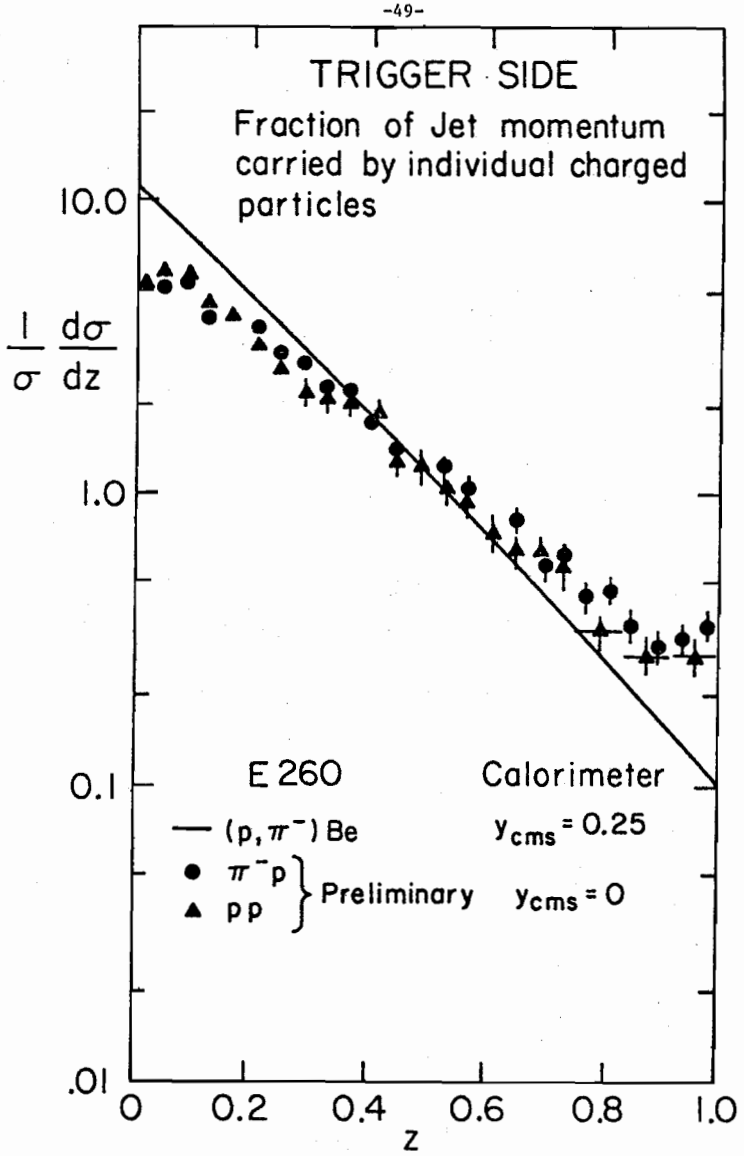

Figure 18: Comparison of the z distribution shown in Fig. 17 (solid line) with the corresponding E260 data from the later run with an H_2 target and calorimeter centered at cms rapidity zero (Ref. 11). The latter distributions are shown separately for π^- and proton beam and are summed over all jets with $p_\perp > 3$ GeV/c.

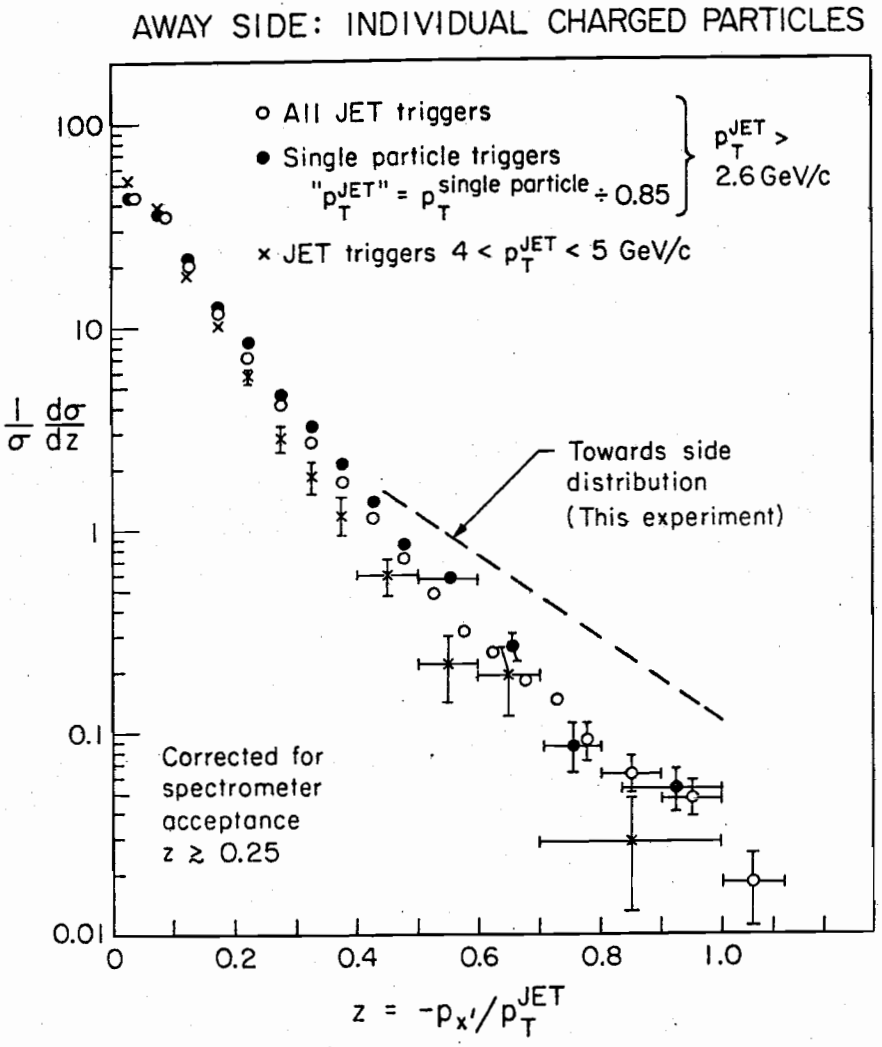

Figure 19: The away side z_J, as defined in Section II, distributions for jet triggers compared to those for single particle triggers. For the latter, we plot $z_J = 0.85\ z_p$. The data are from E260, Ref. 10.

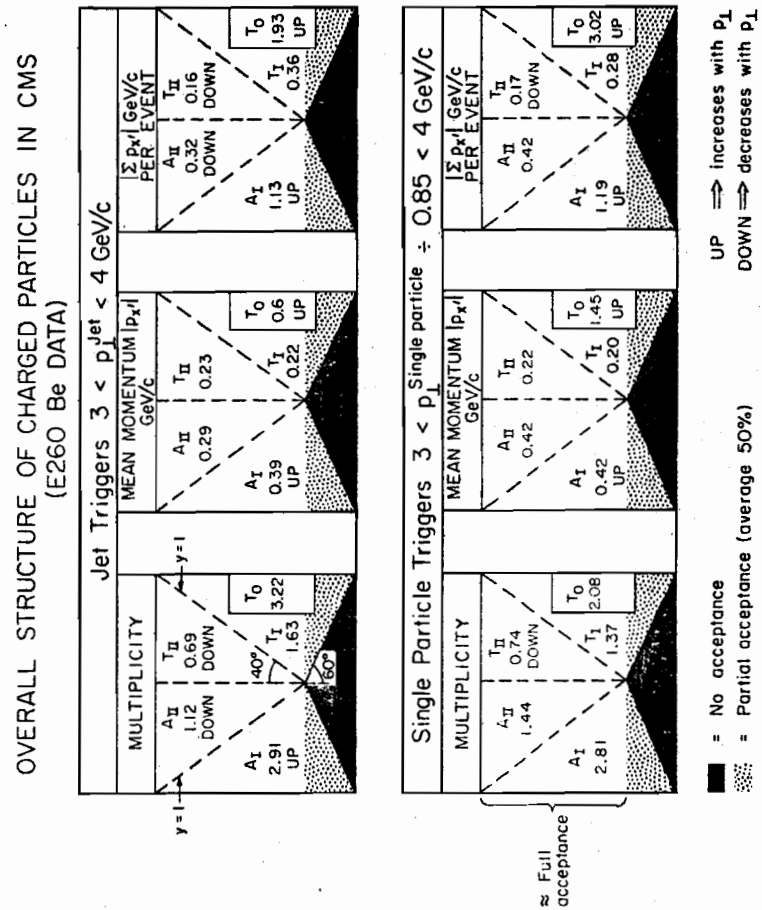

Five regions: T_O (Calorimeter)
T_I Trigger side CMS rapidity y < 1, not into Calorimeter
T_{II} Trigger side y > 1
A_I Away side y < 1
A_{II} Away side y > 1

Figure 20: Distribution of charged particles in five kinematic regions defined in the figure. Plotted is the mean multiplicity, the mean x' component of momentum and their product $|_{region}\langle p_{x'}\rangle|$. Data are given for jet and single particle triggers. Where it is statistically clear, the $p_\perp$ dependence is indicated; more data may be found in Ref. 10 (E260). The figure gives a schematic representation of the E260 acceptance for charged particles.

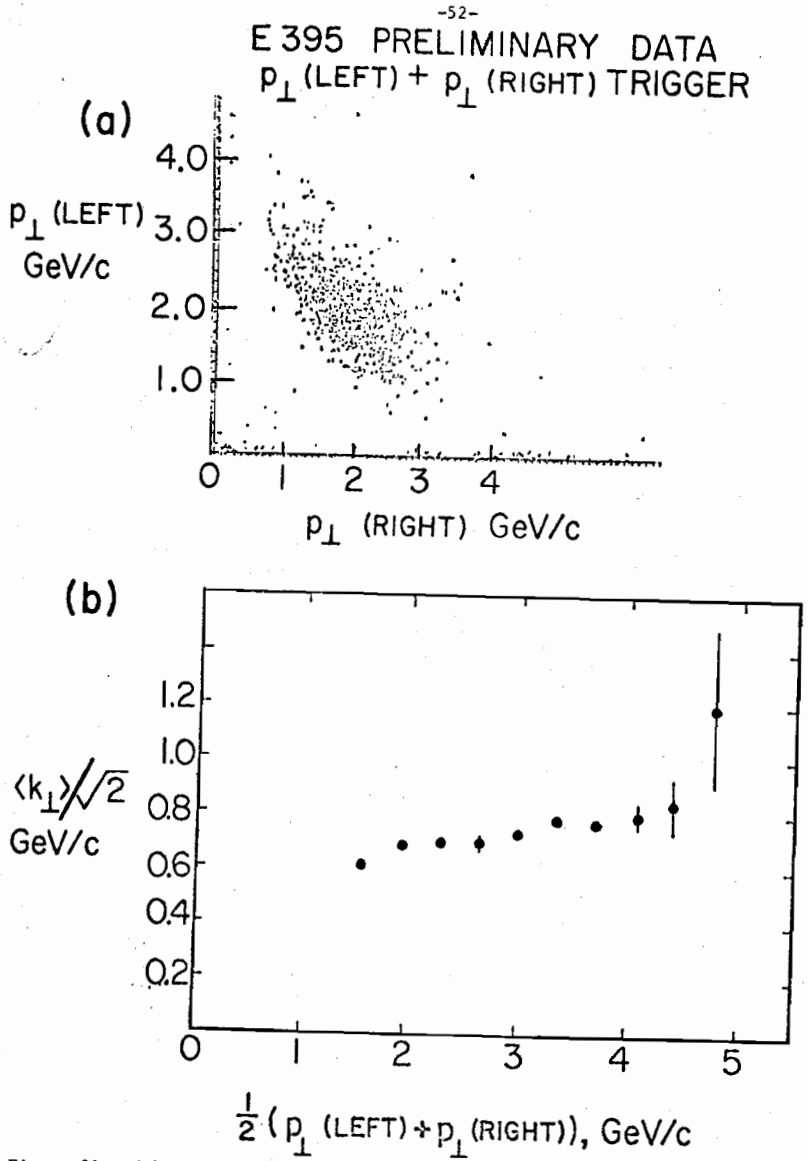

Figure 21: (a) Scatterplot of $p_\perp$ in the right versus that in the left calorimeter for the summed trigger $p_\perp$(left) + $p_\perp$(right) > 4 GeV/c. (b) Plot of $\langle k_\perp \rangle/\sqrt{2}$, where $\langle k_\perp \rangle$ is mean transverse momentum of constituent inside proton, versus trigger $p_\perp$. $\langle k_\perp \rangle$ is found from width of $|p_\perp(\text{left}) - p_\perp(\text{right})|$ distribution in plots like that shown in (a). These data are from E395 (Ref. 12).

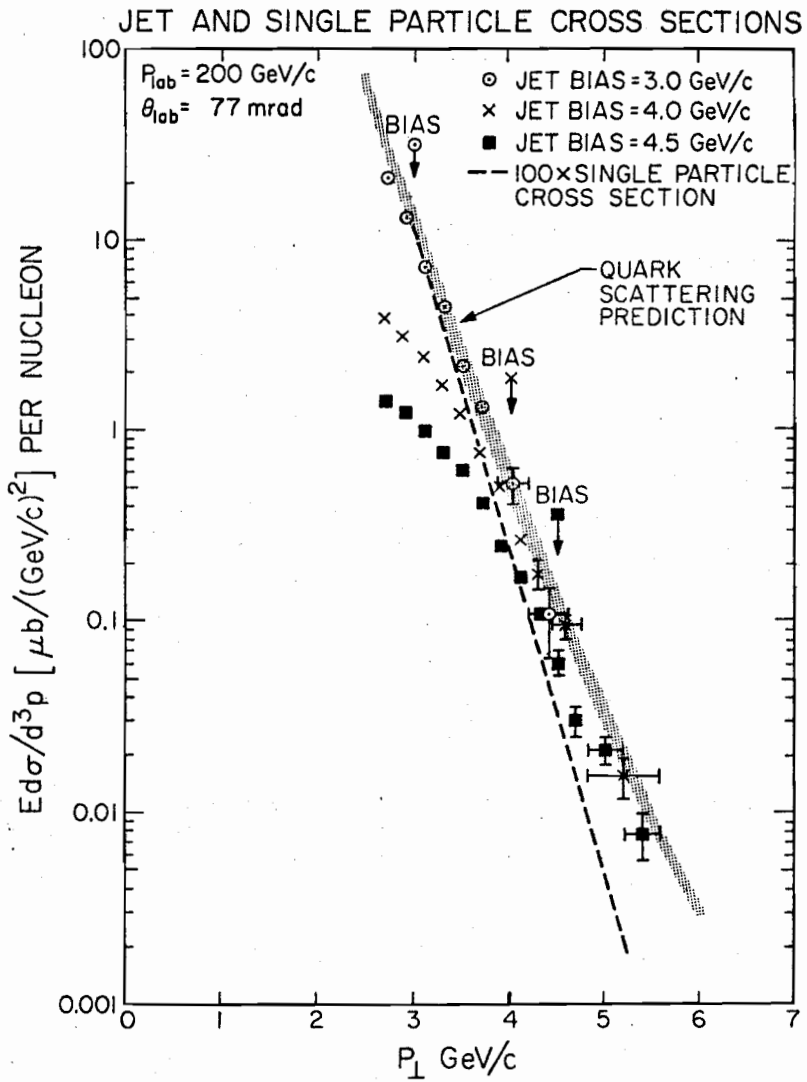

Figure 22: The jet cross-section at 200 GeV/c from E260 (Ref. 10) compared with the prediction of FFF (marked quark scattering, Ref. 32) and the dashed curve which is 100 times the single particle cross-section, summed over <u>all</u> charged particles[1] ($\pi^\pm$ $K^\pm$ $p\bar{p}$). The jet data are averaged over an equal amount of π^- and proton beams while the single particle data have a proton beam. Both sets of data are off a Beryllium target. Note that the plotted data do not possess a very sharp turn on at the calorimeter threshold. This is mainly due to the fact that resolution is improved on an event by event basis by using spectrometer measurement of the charged particles.

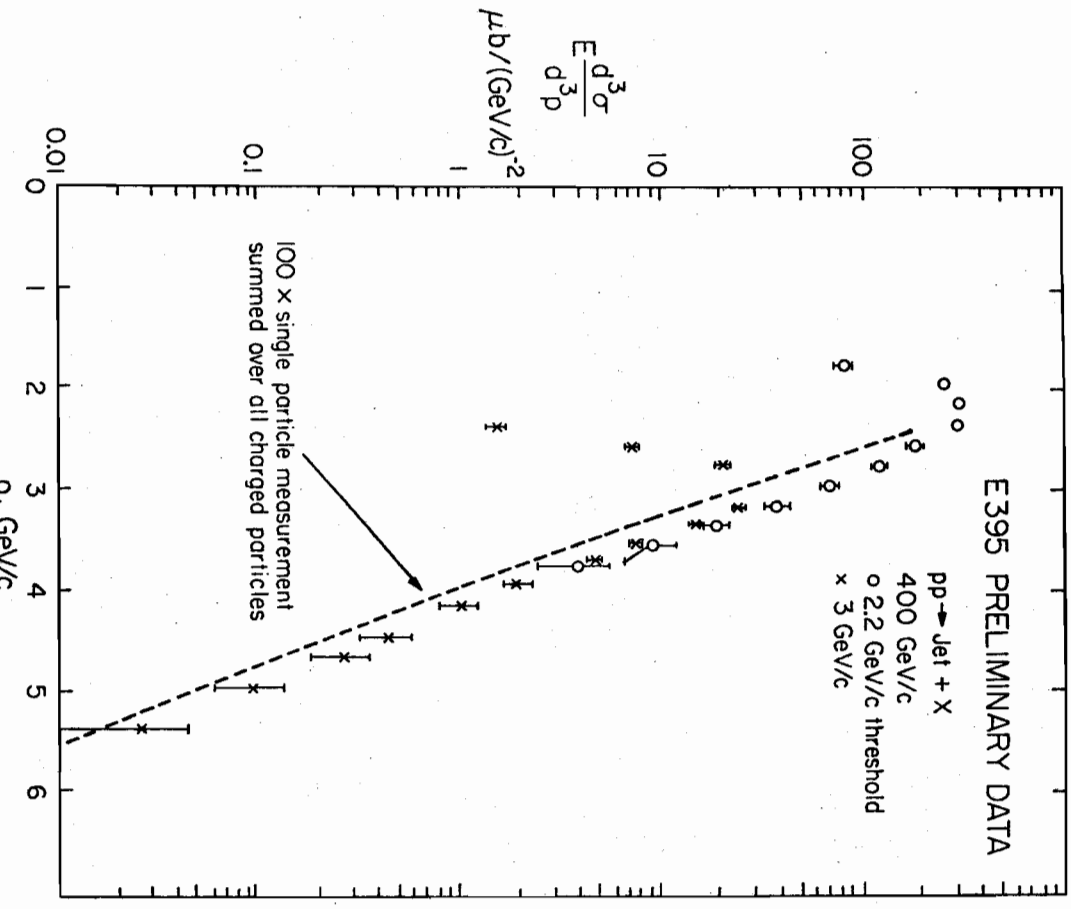

Figure 23: The jet cross-section at 400 GeV/c from E395 (Ref. 12) compared with 100x times the single particle cross-section[1] defined as in Fig. 22 as the sum over all charged particles. Both sets of data correspond to pp scattering.

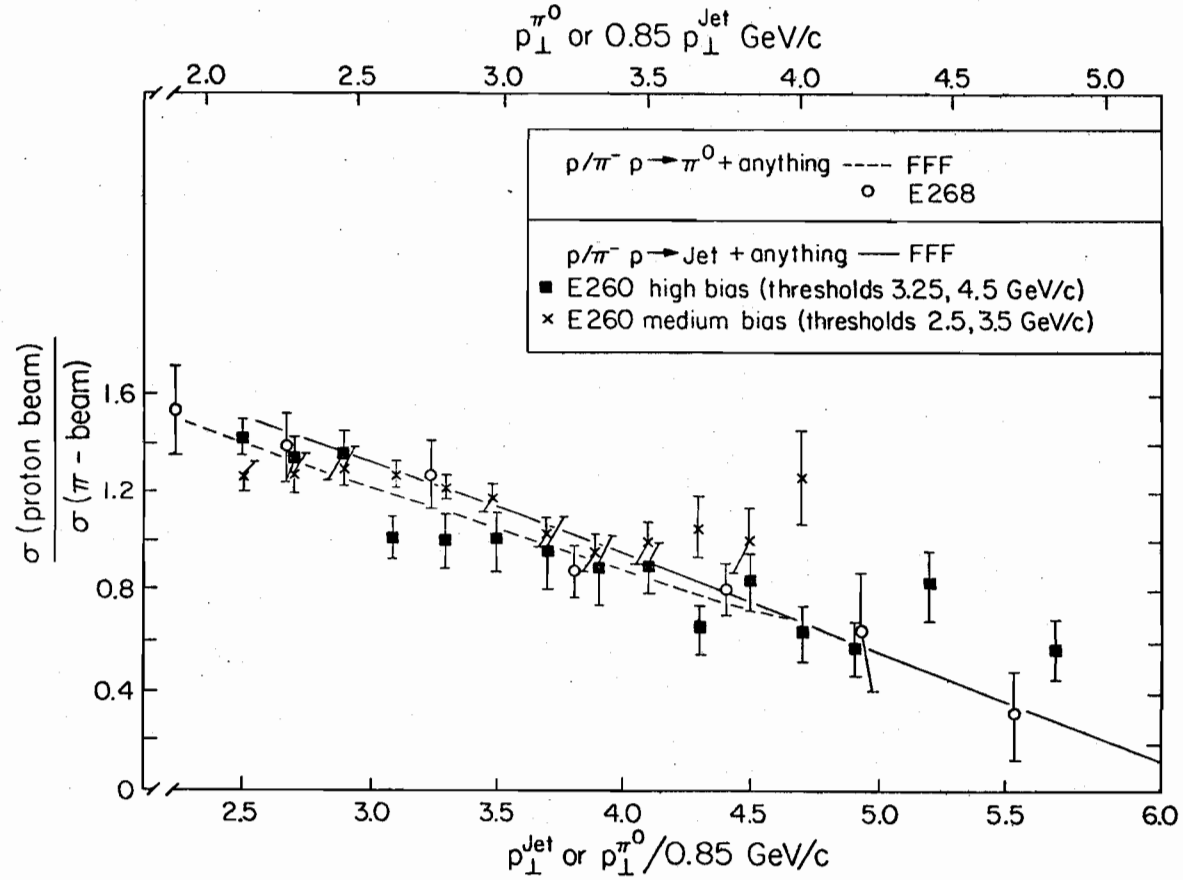

Figure 24: Ratio of the jet cross-sections from π^- and proton beams from E260 (further analysis of data in Ref. 11). It is compared with the similar ratio for single π^0 production taken from Ref. 2. The single particle $p_\perp$ scale is scaled by 1/0.85 for the reason discussed in Section VE. Also shown are the predictions of FFF (Ref. 16).

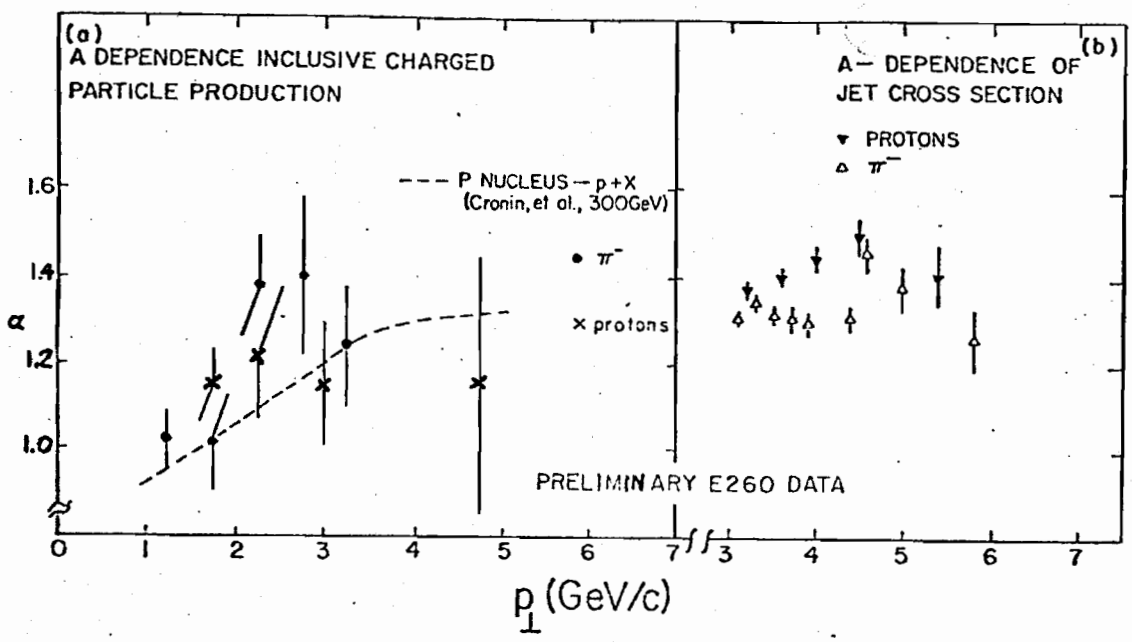

Figure 25: A dependence (parameterized as cross-section per nucleon $\propto A^{\alpha}$) from E260 for jets and single particles (Ref. 11). The single particle data are summed over all charged particles in the final state and are compared with proton production data from Ref. 1. The E260 results are shown separately for a π^- and proton beam.